Climate-driven Variations in Nitrogen Retention from a Riverine Submerged Aquatic Vegetation Meadow

M. Botrel[1,2], C. Hudon[2,3], J. B. Heffernan[4], P. M. Biron[2,5] and R. Maranger[1,2]

[1]Département de sciences biologiques, Université de Montréal, C.P. 6128 succ. Centre-ville, Montréal, QC, Canada.

[2]Groupe de recherche interuniversitaire en limnologie (GRIL).

[3]Environment and Climate Change Canada, Montréal, QC, Canada.

[4]Nicholas School of the Environment, Duke University, Durham, NC, USA

[5]Department of Geography, Planning and Environment, Concordia University, Montréal, QC, Canada.

Corresponding author: Morgan Botrel (morganbotrel@gmail.com)

Key Points:

- Nitrogen retention and biomass were measured at high resolution over six summers in a submerged aquatic vegetation meadow of a large river
- Among the highest riverine nitrate uptake rates were recorded and 47-87% of loads were retained with plants favoring denitrification
- Interannual climate variation influenced nitrate retention by altering water levels, temperature, plant biomass and tributary nitrate load

Abstract

Large rivers can retain a substantial amount of nitrogen (N), particularly in submerged aquatic vegetation (SAV) meadows that may act as disproportionate control points for N retention in rivers. However, the temporal variation of N retention remains unknown since past measurements were snapshots in time. Using high frequency measurements over the summers 2012-2017, we investigated how climate variation influenced N retention in a SAV meadow at the confluence zone of two agricultural tributaries entering the St. Lawrence River. Distinctive combinations of water temperature and level were recorded between years, ranging from extreme hot-low (2012) and cold-high (2017) summers (2 ˚C and 1.4 m interannual range). Using an indicator of SAV biomass, we found that these extreme hot-low and cold-high years had reduced biomass compared to hot summers with intermediate levels. In addition, change in main stem water levels were asynchronous with the tributary discharges that controlled NO_3^- inputs at the confluence. We estimated daily N uptake rates from a moored NO_3^- sensor, and partitioned these into assimilatory and dissimilatory pathways. Measured rates were variable but among the highest reported in rivers (median 576 mg N m^{-2} d^{-1}, range 60 – 3893 mg N m^{-2} d^{-1}) and SAV biomass promoted greater proportional retention and permanent N loss through denitrification. We estimated that the SAV meadow could retain up to 0.8 kt N per year and 87% of N inputs, but this valuable ecosystem service is contingent on how climate variations modulate both N loads and SAV biomass.

Plain Language Summary

Large rivers remove significant amounts of nitrogen pollution generated by humans in waste waters and from fertilizers applied to agricultural lands. Underwater meadows of aquatic plants remove nitrogen particularly well. To keep the river clean, plants use the nitrogen themselves, and promote conditions where bacteria can convert this pollution to a gas typically found in air. Measuring nitrogen removal in rivers is really difficult, and we don’t know how climate conditions influences this removal or plant abundance. We successfully measured nitrogen pollution removal from an underwater plant meadow in a large river over six summers. We found that plant abundance and river nitrogen inputs were critical to determine how much pollution was removed, and that these were controlled by climatic conditions. Plant abundance was controlled by both water temperatures and levels. When water was warm and levels were

neither too high nor too low, conditions were perfect for lots of plants to grow who mainly stimulated bacteria that removed nitrogen. We showed that the amount of nitrogen pollution removed over the summer by the meadow changes with climatic conditions but in general represents the amount produced by a city of half a million people.

1 Introduction

Human activities on land has led to increased delivery of nitrogen (N) to aquatic ecosystems, resulting in the degradation of receiving waters (Carpenter et al., 1998; Galloway et al., 2003). During the transfer from land to sea, these impacts are modulated by river networks that retain a considerable amount of N, either through temporary biotic uptake in the water column or permanent removal by denitrification in anoxic sediments (Hall et al., 2009; Seitzinger et al., 2006). Within hydrographic networks, modelling efforts suggest that large rivers have a substantial influence on basin-wide N retention (Seitzinger et al., 2002; Wollheim et al., 2006; Ye et al., 2017). This influence is explained by their broader reaches that increase water residence time and contact rate with reactive surfaces, combined with higher N loads due to their downstream position. However, N retention in rivers is highly heterogeneous (Piña-Ochoa & Álvarez-Cobelas, 2006) and specific locations, like submerged aquatic vegetation (SAV) meadows, can display a disproportionate retention, thus acting as control points (Bernhardt et al., 2017, e.g. Pinardi et al., 2009; Preiner et al., 2020).

This disproportionate role of SAV meadows can be explained by a suite of positive feedbacks enhancing plant growth and N uptake. For example, SAV reduce flow velocities and increase water transparency through sediment deposition (Hilt, 2015; Scheffer et al., 1993). The role of SAV in N dynamics might be amplified by their location within rivers. For example, high N retention has been observed in a meadow located in a confluence zone of one river (Hudon & Carignan, 2008), but near undetectable denitrification rates were reported at one located in the main channel of another (Tall et al., 2011). This might be due to the specific geomorphologies, like deltas, at confluence zones that increase water residence time and favors N retention in comparison to the higher velocities in main channels. Greater N retention at confluence zones can also be explained by their typically high productivity caused by the increased nutrient supply from incoming tributaries (Benda et al., 2004; Rice et al., 2008). Nevertheless, information on the effect of SAV on N dynamics in rivers remain scarce, with only a handful of studies addressing the topic in rivers with discharges greater than 100 $m^3 s^{-1}$ (Diamond et al., 2021; Hudon & Carignan, 2008; Hudon et al., 2017; Tall et al., 2011) and a few in rivers with discharge of less than 20 $m^3 s^{-1}$ (Audet et al., 2021; Desmet et al., 2011; Heffernan & Cohen, 2010; Pinardi et al., 2009; Preiner et al., 2020). As a result, we have some understanding, albeit fragmented, of N dynamics in SAV meadows across rivers. Yet, past evidences are snapshots

over a day, a season, or a year at most, and do not capture the temporal variability in N retention imposed by climate.

Indeed, N retention fluctuates among years as a function of climate variations as shown by previous studies relating net human watershed N input to riverine exports (Ballard et al., 2019; Goyette et al., 2019; Howarth et al., 2012). In temperate regions, water flow (levels or discharge) and temperature tend to be negatively correlated because of higher evapotranspiration of land plants with increased temperatures (e.g. Hudon et al., 2010). As a result, colder than average growing seasons should exhibit higher runoff watershed losses, faster within-river flow, and consequently increased N export. In contrast, warmer growing seasons should result in lower discharge and higher N retention through enhanced plant and microbial activity, potentially compounded by lower precipitation and higher water residence times. However, the effect of climate and temperature variation on riverine SAV dynamics and overall N retention remains unknown. Rising temperatures can affect SAV biomass either by directly increasing growth rate (Brown et al., 2004; Farquhar et al., 1980) or by improving light availability through water level decline. During extreme drought, water levels can go below a deleterious threshold after which air exposure can lead to the dry-out of above ground biomass (Ersoy et al., 2020; Hudon et al., 2010). Growth rates could also increase to a temperature optimum where SAV thereafter could be outcompeted by periphyton or phytoplankton (Short et al., 2016), which may result in a decrease in N retention through reduced reactive surfaces and higher flow velocities. As SAV meadows in rivers represent a potential control point for N loss, characterizing how climate variations influence this critical ecosystem service is of high importance.

Accurate estimates of N loss in large rivers are particularly challenging because methods for measuring SAV biomass and N retention throughout or over multiple growing seasons are restricted and time consuming. Capturing changes in SAV biomass over a growing season requires the processing of many plant samples, or in typically turbid waters, conducting numerous remote sensing surveys using a sonar (Botrel et al., 2022). One potential solution to track temporal SAV biomass is to use the difference in slope in surface water level between gauging stations around large riverine meadows. Variations in water level slope tend to follow plant development because as SAV accrues biomass, flow is obstructed by the biomass in large meadows resulting in an increase surface water elevation upstream (Boudreau et al., 1994). This approach has been used successfully to estimate biomass in a large river (Giacomazzo et al.,

2020; Vis et al., 2007). As for N uptake measurements, few reliable methods exist in large rivers. The typical isotopic or nutrient release experiments used to measure N uptake rates in streams are impractical in large rivers because of the enormous quantities of injected N needed to detect and track a downstream signal in a large water mass (e.g. Mulholland et al., 2002; Newbold et al., 1981; Peterson et al., 2001). Consequently, past N uptake estimates in large rivers are very coarse as they were either derived from large scale mass balance (Alexander et al., 2000; Howarth et al., 1996) or from models that upscaled measurements taken in small streams (Hall et al., 2013; Wollheim et al., 2006; Ye et al., 2017). However, the development of in situ high frequency NO_3^- sensors provides a unique opportunity to directly measure variation in N uptake rates, particularly in rivers subjected to human derived N inputs where NO_3^- is typically the dominant N form (Caraco & Cole, 1999). Using these sensors, N uptake can be estimated daily by a passive mass balance between two stations along a river reach. Furthermore, when autochthonous primary production is high, NO_3^- concentrations tend to display a diel variation driven by daily change in sunlight and gross primary productivity (GPP) that can be used to estimate autotrophic NO_3^- uptake (Hall et al., 2009; Heffernan & Cohen, 2010). As a result, high frequency NO_3^- signals allow for the partitioning of total N uptake rates into assimilatory and dissimilatory pathways, providing additional information on N fate.

Given the lack of knowledge on temporal N retention dynamics in riverine SAV bed, our objective is to characterize how interannual climate variation affects N retention in a large riverine SAV meadow located at a confluence zone. We hypothesized that retention would be a function of NO_3^- loads and of vegetation biomass, both of which are related to climate-driven variations. To do so, we estimated SAV biomass and environmental conditions over six summers in a natural widening of the St. Lawrence River (SLR), a large temperate river with seasonal ice cover. Using a passive mass balance approach with an in situ sensor, we contrasted interannual variations of N retention within the flow path of the SAV meadow and partitioned retention into autotrophic assimilation and denitrification. N retention was then upscaled to the entire SAV bed using a simple regression model.

2 Materials and Methods

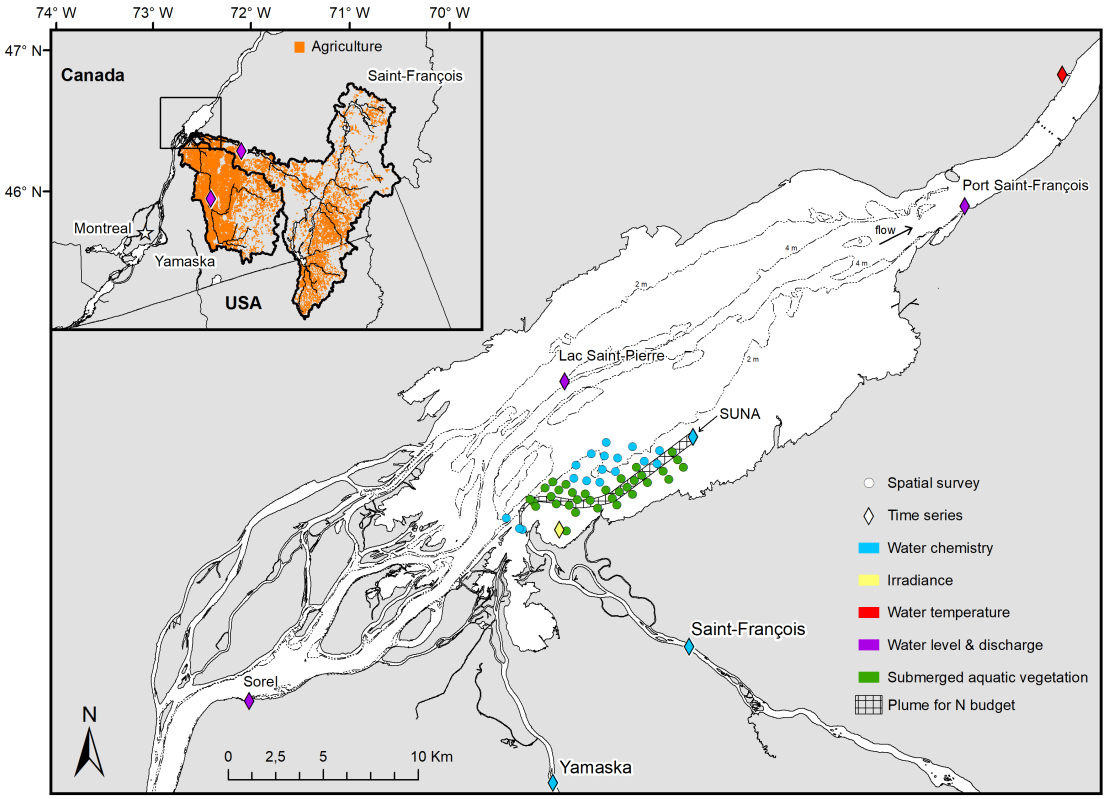

Figure 1. Map of the study area and site locations in Lake Saint-Pierre. The limits of Yamaska and Saint-François river watersheds (thick outline) and farmlands (orange) are delineated and the frame indicates the location of the enlarged area (inset). The dotted lines in the lake are the 2 m and 4 m isobaths. Notice that tributaries gauging stations are only shown in inset.

2.1 Study Site

We studied N retention in a large (~10 km^2) SAV meadow receiving waters at the confluence of two agriculturally impacted rivers (Goyette et al., 2016), the Saint-François (10.18 x 10^3 km^2, 2012-2017 median summer discharge = 74 m^3s^{-1}) and the Yamaska (4.45 x 10^3 km^2, 20 m^3s^{-1}). At the same location, these two tributaries join the fluvial Lake Saint-Pierre (LSP), a ~ 400 km^2 shallow widening (mean depth of 3 m) of the St. Lawrence River (SLR, 8th order, 9640 m^3/s), Québec (Canada, Figure 1). Annual loads of total N from the Yamaska (7.03 x 10^3 tons yr^{-1}) far exceeded those of the Saint-François River (4.45 x 10^3 tons yr^{-1}), in spite of its much

smaller watershed (Hudon et al., 2017). The impact of intensive farming on the Yamaska drainage basin was also shown by its high conductivity and high flashiness after local rain events. Conductivity in the tributaries is distinct (median, $med_{Saint\text{-}François}$ = 370 µS cm^{-1}, $med_{Yamaska}$ = 206 µS cm^{-1}), allowing for its use as a conservative tracer of water mass.

Located at the mouth of their confluence with the SLR, the SAV meadow under study was well positioned to intercept and filter the nutrient-rich waters from both tributaries, as was previously suggested by a nutrient mass balance study in LSP (Hudon & Carignan, 2008). Lake Saint-Pierre supports about half of the remaining SLR wetlands (Hudon et al., 2018; Jean et al., 2002), and has been designated as both a Ramsar site and a UNESCO biosphere reserve. Although its natural capital has been recognized, LSP hydrodynamics have been highly modified by human activities. Discharge from the Great Lakes to the SLR is regulated at the Moses-Saunders dam (Cornwall, ON, Massena, NY), which has resulted in an overall reduction in water level extremes in LSP of 0.7 m on average between 1912 and 1994 (Hudon, 1997; Hudon et al., 2006). The effects of flow regulation have been compounded by the dredging of a 11.3 m-deep navigation channel that focuses water flow from the Great Lakes to the central part of the lake (0.5-1 m s^{-1}, representing 55-88 % of total discharge (Hudon & Carignan, 2008; Morin & Côté, 2003, Figure 1). As a result, flow is markedly slower (< 0.5 m s^{-1}) in the lateral shallow zones particularly during summer, when mixing of incoming tributaries with this central water mass is limited (Vis et al., 2007). Reduction in flow velocity in the lateral zones is also explained by the presence of extensive SAV present up to a maximum depth of 3 m (Hudon, 1997).

While the bulk of SLR flow is controlled anthropogenically, water levels nevertheless follow interannual fluctuations as a function of climate variation. Flow regulation has a stabilizing effect on waters originating from the Great Lakes (772 x 10^3 km^2), which account for approximately 70 % of the SLR waters entering LSP (Hudon et al., 2017). The climate effect is thus primarily the result of tributary inputs, the largest of which is the Ottawa River (146.3 x 10^3 km^2), a North shore tributary accounting for ~20% of water inputs in LSP. The much larger sizes and areas covered by the SLR watershed compared to its individual tributaries further induce a potentially complex influence of climate at their confluence zones. The SLR main stem climate variation is an aggregate of the basin-wide Great Lakes and overall tributaries water inputs, while individual tributaries discharges and NO_3^- concentrations are independent of these large-scale variations and represent localized precipitation patterns.

2.2 Spatial Survey of SAV Biomass and Water Chemistry

Field surveys were carried out during maximum SAV biomass accumulation, around early August from 2012 to 2017, and once during the early growing season in June 2012. We measured SAV biomass at approximately 35 sites. Water temperature and conductivity were measured using a YSI 556 MPS or a YSI 600XL at each site as well as at ~17 additional sites within and around the meadow (Figure 2). SAV was collected every summer using the rake technique, with additional diver-collected quadrats in 2016. For the rake technique, a 0.35 m-wide double-headed rake was lowered in the water and dragged toward the boat over a length of approximately 1 m. In 2016, divers harvested all plant material within a 0.30 m by 0.30 m PVC frame placed on the lake bottom. At each site, 3 to 5 replicates were collected, and plant material was rinsed on-boat, stored in plastic bags, and frozen once on shore. Upon return to the laboratory, plant samples were thawed, wrung out manually, sorted by species, separated from filamentous algae, dried to a constant mass at 60°C, and weighed (0.001g). The sum of species dry biomass in g m^{-2} was calculated per sample and averaged at each site (3-5 replicated) SAV species composition was dominated by *Vallisneria americana* and *Potamogeton richardsonii*, but also included *Heteranthera dubia*, *Stuckenia pectinata*, *Elodea* spp, *Myriophyllum* spp. and *Chara* spp. Because rake biomass collections are underestimated due to loss of plant material during sampling, rake estimates were converted to quadrat equivalency using a previously determined general relationship (Botrel et al., 2022).

2.3 Time Series Data

2.3.1 Temporal SAV Biomass Estimates

Daily SAV biomass was estimated between June and November using the slope in surface water level between gauging stations (Figure 1). Slopes were calculated as water surface elevation upstream minus downstream divided by distance between successive stations (23 km, Supporting information, SI, Text S1). As variations in water level slope are also affected by signals other than SAV growth, such as tides and winds (Vis, 2004), we extracted the SAV signal with the Hilbert-Huang transform method using the hht and EMD packages in R (Bowman & Lees, 2013; Huang et al., 1998; Kim & Oh, 2018; Wu & Huang, 2009). We chose this signal extraction method because it is adaptative and intrinsic, and is entirely based on data without

imposing an a priori hypothesis on the shape of the SAV growth curve (Wu et al., 2007). We analyzed water level slopes only during the growing season (June 21 to September 22), therefore SAV signal corresponded to the EMD residuals or the seasonal trend. To reduced signals mixing at different time scales (i.e. mode mixing), we used a noise-assisted version of EMD, ensemble empirical mode decomposition (EEMD, Bekka & Berrouche, 2013). Confidence levels were estimated to assess between year differences using the bootstrapping approach of Ezer & Corlett (2012, SI Text S1).

To reconstruct SAV growth using changes in water level slopes as an indicator of daily biomass, we assessed the optimal gauging station representative of SAV biomass. For this validation, we used the Pearson correlation between the slope signal to the overall biomass measured during spatial surveys (SI Text S1 and Figure S1). The slope calculated between the downstream gauging stations (Port St-François) to the middle LSP station yielded a higher correlation ($r = 0.98$) than the slope between upstream Sorel station and the same middle station ($r = 0.33$). Using this former slope value and to provide estimates using a common metric, we calculated maximum summer SAV biomass using a simple linear regression between rake estimated biomass and slopes ($r^2 = 0.97$, $p < 0.0001$). For visualization of SAV growth patterns and statistical analysis, we directly used the slope between the Port St-François and LSP station as an indicator of temporal SAV biomass changes.

2.3.2 Nutrient Inputs

To estimate daily NO_3^-, total phosphorus (TP) and turbidity in the tributaries, we used the composite approach from the R package loadflex that includes regression modelling with discharge as a predictor and a residual correction (Appling et al., 2015). The best regression models were selected using Akaike information criterion (AIC) from among 9 models fitted for data between 2009 and 2018 in the rloadest package (Johnson & Omland, 2004; Runkel & De Cicco, 2017). Weekly water chemistry data from both provincial and national agencies collected in the Saint-François and Yamaska rivers (Table S1) were used to derive models. To avoid autocorrelation when fitting models, a subset of data at time intervals greater than 7 days was used; the complete dataset was used for the residual correction. Daily discharge data was acquired at upstream stations in Drummondville for Saint-François and Saint-Hyacinthe for Yamaska (Table S1). Missing data (3 days) from Saint-François were filled using data available

from a station 1 km upstream, Hemming Falls (r = 0.93), while missing data from the Yamaska dataset (22 days) were filled using the linear regression between daily discharge at Saint-Hyacinthe and the sum of discharges at the two main upstream sub-watershed stations (Farnham and Noire, R^2 = 0.96).

Water chemistry monitoring stations were located near the mouth of the tributaries, but discharge stations were located 47 km and 63.5 km upstream for Saint-François and Yamaska respectively. Discharge was corrected for additional water inflow using the pro-rate technique and was multiplied by the proportional increase in drainage area at the respective water chemistry stations (1.05 and 1.34 for Saint-François and Yamaska, Morse, 1990). We also corrected daily discharge according to transit time estimated with Saint-Venant equations which included information on channel geometry and friction coefficients (P. Fortin ECCC pers. comm.). During summer (from June 21 to September 22), transit time was longer than 24h for 4% and 65% of dates for Saint-François and Yamaska respectively. Longer transit times in Yamaska were probably due to its smaller watershed size and the higher distance between the gauging station to the river mouth. To describe total tributary inputs during the SAV growing season, discharges are reported as the sum of both tributaries. Summertime concentrations received by the SAV bed were weighted by the proportion of individual tributary (i) discharge to the total discharge ($[NO_3^-]$ (mg L^{-1}) = $\sum_i^2([NO_3^-]_i \times {}^{Q_i}/_{Q_{total}})$).

2.3.3 Downstream NO_3^-, Temperature and Light Estimates

To estimate NO_3^- concentrations downstream of the SAV meadow, a SUNA V1 sensor (Satlantic) using in situ ultraviolet absorption spectroscopy (200-400 nm spectra) was moored from the end of June to end of September in 2012 to 2016 (Figure 2). The sensor, equipped with a battery pack, flow cell, and a Sea-Bird electronic pump, was mounted on an aluminum stepladder which kept the sensor at 75 cm above the sediment. Before and after moorings, calibration was verified using distilled water and known NO_3^- concentrations. To limit the interference of large particles on the ultraviolet lamp, a pre-filter with a mesh size of 5 mm was installed at the water intake. Each hour, water was pumped, and four measures were recorded. Only measurements within manufacturer-specified accuracy (+- 0.028 mg N L^{-1}) were deemed acceptable and median values were kept for further analysis. A sensor to measure hourly

dissolved oxygen concentrations (D-Opto) was also deployed in 2016, with punctual measurements over other years.

Continuous local water temperature was taken from the SUNA sensor, and validated with D-Opto measurements in 2016 (r = 0.99). Additional water temperature time series were acquired at Trois-Rivières station (Table S1) and correlated with daily water temperature measured by the SUNA and mean water temperatures measured during spatial surveys (r = 0.72 and r = 0.75, respectively). Hourly short-wave radiation was acquired from NASA datarod at a location close to the SAV bed (46.1247 N, 72.9018 W, Teng et al., 2016, apps.hydroshare.org/apps/data-rods-explorer). Short-wave radiation flux (300-2000 nm in Wm^{-2}) was converted to photosynthetically active radiation (PAR, 400-700 nm) in photon flux density units (mol m^{-2} h^{-1}) using a conversion ratio of 2.114 (Britton & Dodd, 1976). To describe SAV growing season, we calculated the accumulated degree days using a reference temperature of 7°C, which corresponds to the known sprouting temperature of *Vallisneria americana* (Lacoul & Freedman, 2006), a common species at our study site. Similarly, cumulative PAR was calculated as the sum of daytime hourly irradiance.

2.3.4 NO_3^- Budget and Fate

We calculated a nitrate (NO_3^-) budget for a plume spanning from the mouths of the tributaries (input) to the downstream edge of the SAV meadow where the SUNA was located (output, Figure 1). NO_3^- was the dominant N form in these tributaries (60 % on average) and is a significant agricultural pollutant. A complete summary of equations used to derive budgets is presented in Table 1. The shape of the plume was drawn from trajectories of drifters deployed in 2005, 2006 and 2012 (SI Figure S1). A plume width of 500 m was used for calculations, corresponding to the distance between stations of the spatial survey and was chosen based on conductivity measurements as a conservative tracer of water masses. When choosing the location for the outflow station in 2012, the objective was to measure NO_3^- from the Saint-François water mass flowing through the SAV bed. Since 2012 was an extremely low water level year, the sensor was placed at the offshore limit of this water mass to ensure water was deep enough to allow measurements throughout the summer. However, the study area is a complex zone at a confluence of the Saint-François and Yamaska rivers. Based on delineation using optical properties from satellite observations (pers. comm. P. Massicotte) and conductivity, we observed

that in subsequent higher water level years, the same outflow location was most likely exposed to a mixture of waters from both rivers. Daily upstream NO_3^- concentrations were thus estimated from the NO_3^- loadflex predictions multiplied by the contribution of Saint-François and Yamaska to the water flowing at the downstream site (Table 1, equation 1). To estimate contributions, we used a two end member mixing model with conductivity as the conservative tracer and applied an analytical solution (Table 1, equation 2). Contributions were estimated once per summer using matching monthly conductivity at the nearest sampling station to the SUNA and conductivity measurements in the tributaries from this study and the provincial monitoring station (Table S1).

Daily discharge at the outflow site was computed as the area of the plume cross-sectional transect multiplied by flow velocity (Table 1, equation 3). The cross-sectional area was estimated from the sum of cell depths measured for the outflow transect on a bathymetric raster map (Hudon & Carignan, 2008), corrected for daily water level height, and multiplied by the bathymetric cell width. Daily velocity was estimated from Delft3D simulations, a tridimensional hydrodynamic model established for our study area (Bulat et al., 2019). Model simulations were run for each year using median, minimum, and maximum input discharges at Saint-François over the SUNA mooring period, and yearly spatial polygons of SAV height established from SAV echosounding surveys (Botrel et al., 2022). Mean depth average velocity was computed on the resulting spatial polygon grid of 70 m resolution at the outflow transect (7 polygons). Mean residence time was also estimated from depth-averaged velocity assuming a travelling distance of 11.61 km, but the mean was computed over the complete plume surface area. To estimate both daily velocity and daily residence time, interpolations were computed using yearly linear regressions between daily Saint-François discharge and the mean depth average velocities or the mean residence time (i.e. Delft3D inputs and outputs).

Daily total areal uptake (U_t) was considered to be the sum of daily autotrophic assimilation (U_a), denitrification (U_d), and heterotrophic assimilation (U_h, Table 1, equation 4). U_t was calculated as the difference in daily median outflow NO_3^- concentration between upstream input and output (downstream) while taking residence time into account, multiplied by the ratio of outflow discharge divided by the plume area (Table 1, equation 5). Daily proportional uptake (R) was calculated as the median NO_3^- concentration at the outflow minus upstream inputs, divided by those inputs (Table 1, equation 6). U_a was calculated from diel NO_3^-

variation using equation 7, Table 1, and U_d as the difference between U_t and U_a. Since hourly NO_3^- data at the downstream station was a composite of multiple frequency signals, we extracted diel variations using Hilbert-Huang transform, similar to the SAV time series and to the protocol of Chamberlin et al. (2021). This method is best suited for nonstationary data, a common feature of hydrological time series (Lloyd et al., 2014). Days for which more than five consecutive hourly measurements were missing were excluded from the data series (5 days in 2012 and 2013, 1 day in 2014), otherwise missing values were linearly interpolated. For our five NO_3- time series (2012-2016), IMF4 always corresponded to the diel signal with mean instantaneous periods between 21 and 23 hours. When a NO_3^- spike introduced oscillations on the diel IMFs (Stallone et al., 2020), those sections were removed from the analysis. We then filtered the resulting U_a to obtain time intervals between daily maximums of 20 to 28 hours.

U_a estimated from NO_3^- time series were validated to autotrophic assimilation estimates based on gross primary production ($U_{a\text{-}GPP}$) calculated from the oxygen time series in 2016 (equation 8). For this $U_{a\text{-}GPP}$ calculation, we assumed a photosynthetic coefficient of 1, an autotrophic respiratory coefficient of 0.5, and used a mean C : N ratio measured for both SAV and macroalgae in LSP (molar ratio of 13 : 1). Daily gross primary production (GPP) and ecosystem respiration (ER) were calculated using the bookkeeping method in the R package LakeMetabolizer (Winslow et al. 2016). For gas exchange estimation, the depth of the surface mixed layer was assumed to be the depth at the outflow site, and oxygen saturation was calculated using in situ water temperature, and atmospheric pressure estimates at the Nicolet weather station. The coefficient of gas exchange was computed using wind speed (Cole and Caraco (1998) estimates from LSP weather station or, when data were missing, from Nicolet (Table S1). Nighttime and daytime periods were estimated using the R package suncalc (Thieurmel & Elmarhraoui, 2019). Validation of the estimates showed that U_a and $U_{a\text{-}GPP}$ were comparable, as most values fell along the 1:1 line and overall means were similar (SI Figure S3). Ecosystemic respiration estimates also allowed for calculation of U_h for 2016, assuming a heterotrophic growth efficiency of 0.2 and molar C : N ratio of 20 : 1 (Table 1, equation 9, Hall & Tank, 2003; Heffernan & Cohen, 2010). As U_h represented less than 0.05% of U_t, this term was considered negligible and was not considered in denitrification estimates. Finally, to isolate the effect of biotic activity on retention (Wollheim et al., 2006; Stream Solute Workshop, 1990), we calculated the uptake velocity (V_f), or the mass transfer coefficient from water to the benthos

(Table 1, equation 10). We calculated both total ($V_{f\text{-}t}$) and process-specific velocity (for autotrophic assimilation $V_{f\text{-}a}$ and denitrification $V_{f\text{-}d}$).

2.4 Statistical Analysis

We used linear discriminant analysis (LDA) to assess the occurrence of among-year differences in environmental variables and N budget during summertime, and to identify which variables generated those differences. Given the smaller number of observations for process-specific rates (*n* total uptake = 292, *n* process-specific = 99), interannual differences were assessed using nonparametric Kruskall-Wallis tests. A principal component analysis (PCA) was used to describe correlations between NO_3^- budget terms and environmental variables. We then determined predictors of U_t using a regression approach. As our data were nested per year and displayed temporal autocorrelation, we conducted regressions as linear mixed models. To find optimal model structures, we applied the protocol of Zuur et al. (2009). We first removed collinear variables and kept the variables that were most correlated to our response variable, U_t. We then selected random effects using a fixed structure of all possible covariates with restricted maximum likelihood estimation (REML). The best model was selected to minimize the sample-corrected Akaike Information Criterion (AICc). Using this optimal random structure, fixed effects were similarly selected using AICc but with maximum likelihood estimation (ML). The final model was fitted using REML and validated for normality and homogeneity by visual inspections of standardized residuals against fitted values and explanatory variables. Using the fixed component of the mixed model, daily retention was predicted from the weighted discharge estimates of NO_3^- concentrations inputs as the explanatory variable. Total summertime retention was estimated by multiplying these predictions with the SAV meadow area (10 km^2) and summing these daily values. Similarly, we estimated total NO_3^- inputs by summing daily loads from the two tributaries. All statistical analyses were conducted in R (RCoreTeam, 2020) using the MASS package for LDA, vegan for PCA and nlme for linear models (Oksanen et al., 2020; Pinheiro et al., 2020; Venables & Ripley, 2002). Prior to analysis, data were transformed when necessary to satisfy normality and homoscedasticity assumptions.

401 **Table 1.** List of Equations Used for Nitrate Budget Calculations. No. equation number. In the
402 'Abbreviated description' column, abbreviations that are used in subsequent equations are only
403 described once in sequential order.

No	Equations	Abbreviated description
1	$[\mathbf{NO_3^-}]_{\mathbf{in}}\ (\mathrm{mg\ L^{-1}}) = [NO_3^-]_{StF} \times f_{StF} + [NO_3^-]_{Yam} \times f_{Yam}$	**Nitrate input ($[NO3\text{-}]_{in}$)**: StF Saint-François River, Yam, Yamaska River, f fraction where $f_{Stf} + f_{Yam} = 1$
2[a]	$\mathbf{f_{StF}} = {(C_{out} - C_{Yam})}/{(C_{StF} - C_{Yam})}$	**Fraction of Saint-François River water mass (f_{Stf})**: out outflow, C conductivity
3	$\mathbf{Q_{out}}\ (\mathrm{m^3 s^{-1}}) = (\sum_{i=1}^{n} h_{out,i} \times w_i) \times u_{out}$	**Discharge at outflow (Q_{out})**: h depth, i ith bathymetric raster cell, w width, u depth average velocity
4	$\mathbf{U_t}\ (\mathrm{mgN\ m^{-2} d^{-1}}) = U_a + U_d + U_h$	**Total nitrate uptake rate (U_t)**: U_a autotrophic assimilation, U_d denitrification, U_h heterotrophic assimilation
5	$\mathbf{U_t}\ (\mathrm{mgN\ m^{-2} d^{-1}}) = \frac{Q_{out,d}}{A}([NO_3^-]_{in-\tau} - [NO_3^-]_{out,med})$	**Total nitrate uptake rate (U_t)**: A area of the plume, τ residence time in days, med median
6	$\mathbf{R}\ (\mathrm{unitless}) = 1 - \frac{[NO_3^-]_{out,med}}{[NO_3^-]_{in-\tau}}$	**Proportional retention (R)**
7[b]	$\mathbf{U_a}\ (\mathrm{mgN\ m^{-2} d^{-1}}) = \frac{Q_{out,d}}{A} \sum_{t=hmax0}^{hmax1} ([NO_3^-]_{max\ (hmax0)} - [NO_3^-]_h)$	**Autotrophic assimilation (Ua)**: t time of day, hmax0 hour of first daily NO_3^- maximum, hmax1 hour of last daily NO_3^- maximum, h hour
8[b,c]	$\mathbf{U_{a-GPP}}\ (\mathrm{mgN\ m^{-2} d^{-1}}) = {(GPP \times h \times p \times r_a)}/{C:N}$	**Autrotrophic assimilation from GPP ($U_{a\text{-}GPP}$)**: GPP gross primary productivity, p photosynthetic coefficient, r_a autotrophic respiratory coefficient, C : N carbon to nitrogen ratio
9[b,c]	$\mathbf{U_h}\ (\mathrm{mgN\ m^{-2} d^{-1}}) = {((ER - (r_a \times GPP)) \times HGE)}/{C:N}$	**Hetetrophic assimilation (U_h)**: ER ecosystem respiration, HGE heterotrophic growth efficiency
10[d]	$\mathbf{V_f}\ (\mathrm{m\ d^{-1}}) = {U}/{[NO_3^-]_{out,med}}$	**Uptake velocity (V_f)**: U uptake rate

404 Equations are derived from [a] Phillips & Gregg (2001), [b] Heffernan & Cohen (2010), [c] Hall &
405 Tank (2003), and [d] Ensign and Doyle (2006).

406

3 Results

3.1 Interannual Variation in Environmental Variables and Temporal SAV Biomass

There were strong and significant interannual variations in environmental conditions during the SAV growing seasons (MANOVA, $p < 0.0001$) caused by several variables that varied differently among summers. Variables that contributed to among-year differences were mainly water level, water temperature, tributary discharge, and NO_3^- input concentrations (LDA, SI Table S2). These conditions created a sharp gradient among summers, ranging from hot temperatures with low water levels to cold summers with high water levels. Mean summer water levels and temperatures spanned 1.4 m and 2°C, respectively coinciding with historical extremes in 2012 and 2017 (Figure 2). Exceptionally low water levels and high temperatures were observed in 2012, whereas 2017 coincided with major flooding from the Ottawa River during the spring freshet and sustained high discharge throughout the season. The other four years, either tended to be hot with low water levels (2016) or had intermediate water levels (0.69 to 0.77 m CD) but varying mean water temperatures (2013, 2014, 2015). In these latter years, 2014 was colder, both in mean temperature (21°C) and accumulated degree day (Figure 2b). For the remaining two years (2013, 2015), the mean temperatures were similar. However, the greater variability in daily temperatures with sporadic colder days in 2013 (min_{2013} = 17°C, min_{2015} = 18.8°C, SI Figure S4) resulted in a lower accumulated degree day that year compared to 2015.

Hotter years (2012, 2015, 2016), with both higher accumulated degree days and mean water temperature, tended to receive more PAR than colder years, but this was not always the case. For example, the second hottest summer (2016) had similar irradiance levels to the two coldest ones (2014, 2017). Whereas mean water temperature and water levels followed a pattern of negative correlation in the SLR, there was no correlation between SLR temperatures and tributary variables (Figure 2e-g). This suggests that tributary loadings were influenced asynchronously from flow patterns in the mainstem. Tributary discharge and weighted NO_3^- had similar patterns albeit NO_3^- concentrations were markedly lower in 2012 as compared to other years (med_{2012} = 0.26 mg N L^{-1}, med_{other} = 0.46-0.72 mg N L^{-1}). This was a function of more variable NO_3^- and considerably higher concentrations in the Yamaska as compared to the Saint-François since its proportion to total discharge stayed relatively stable throughout the different summers (med_{all} = 0.20, med_{year} 0.27 to 0.13, SI Figure S5). NO_3^- concentrations from Yamaska

437 were particularly high during the intermediate temperature years (med_{2015} = 1.75 mg L^{-1}, med_{2013}
438 = 1.77 mg L^{-1}, med_{other} = 0.08 to 0.82 mg L^{-1}), up to 5.5 mg L^{-1}. In contrast, TP and turbidity did
439 not show any obvious differences among years, but TP was lower in 2015 (med_{2015} = 30.2 µg P
440 L^{-1}, med_{other} = 33.6 to 44.0 µg P L^{-1}, Figure 2g) and turbidity higher in 2012 (med_{2012} = 17 NTU,
441 med_{other} = 10 to 15 NTU, SI Figure S4) as compared to other years.

442 From our comparison with field biomass estimates, we deemed the downstream LSP
443 water level slope a good indicator of SAV biomass. Looking at the estimated temporal SAV
444 biomass changes throughout the six summers, two patterns of seasonal progression were
445 revealed (Figure 3). The first pattern reflected a reduced SAV biomass reaching its peak earlier
446 during the season (late July to late August). This pattern was observed over both the colder years
447 with high water levels (2013, 2014, 2017) and the hottest year with very low water levels (2012),
448 suggesting that extreme environmental conditions can restrict SAV growth. In addition, three of
449 these four years (all but 2013) experienced lower NO_3^- inputs from tributaries. The second
450 pattern occurred over years of highest SAV biomass, peaking later during the season
451 (September). SAV growth was favored by warm summers (2015, 2016) with intermediate water
452 levels and high NO_3^- inputs. Overall, these observations suggest that maximum SAV biomass
453 could vary following a dome-shaped curve where the optimum coincided with summers of warm
454 temperature, average water levels and abundant nitrate.
455

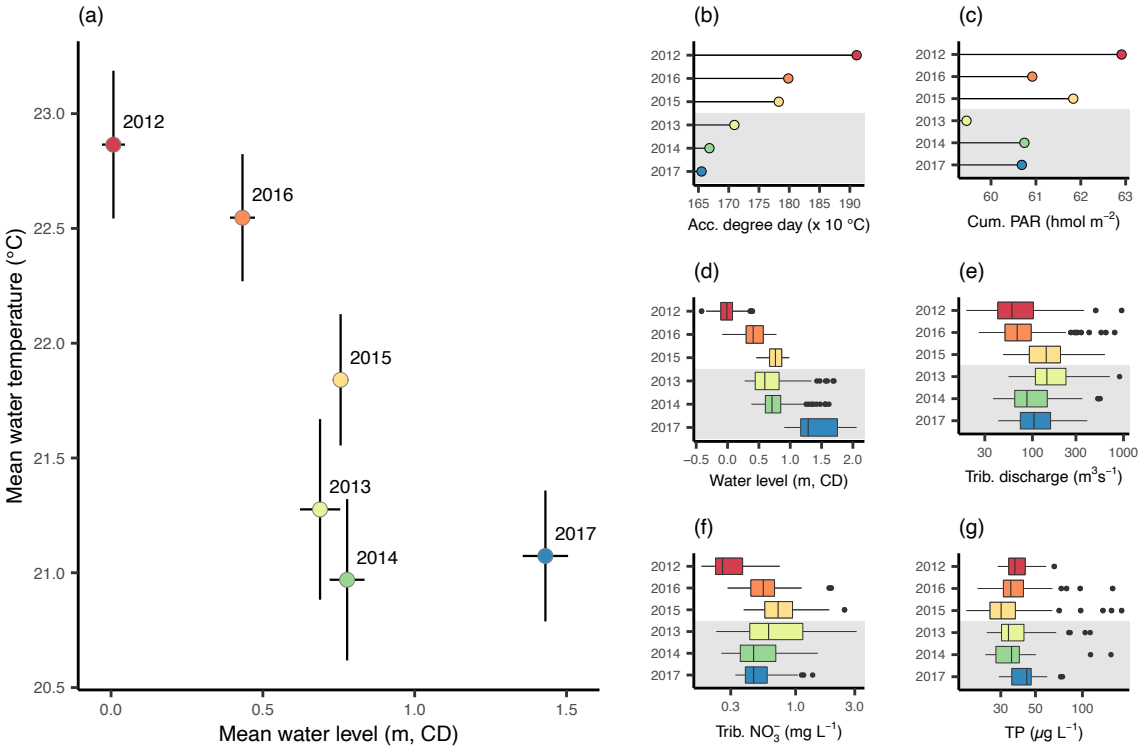

456

457 **Figure 2.** Interannual variation in environmental variables during summers from 2012 to 2017
458 (June 21 to September 22) for the main stem (a-d) and tributaries (e-g). Error bars are 95%
459 confidence intervals around the mean. Dot and boxplots are ordered by decreasing water
460 temperature as accumulated degree day using a warm to cold color gradient; cold summers are
461 indicated by the light grey shaded background. Vertical bars within boxes indicate median value,
462 box boundaries represent 25th and 75th percentile and whiskers range from 10th to 90th
463 percentiles. Cum. cumulative, PAR photosynthetic active radiation, Acc. accumulated, CD Chart
464 Datum, Trib. tributaries. Cumulative summer PAR and degree-days > 7°C were calculated from
465 May 1st to September 22 . Water levels are from LSP station and SLR temperature from Trois-
466 Rivières. Tributaries discharge correspond to the sum of Yamaska and Saint-François discharges.
467 Nitrate and total phosphorus are flow-weighted concentration from the two tributaries.

468

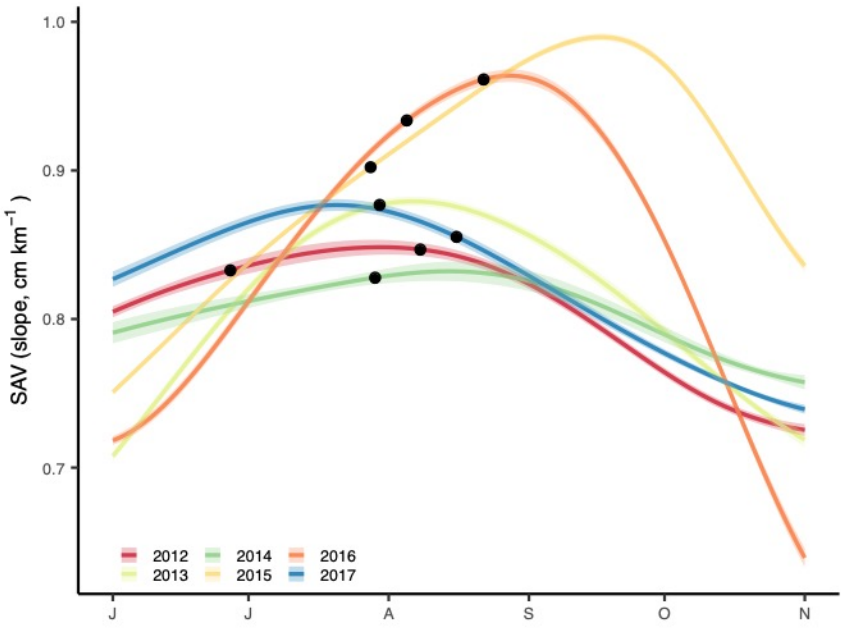

Figure 3. Interannual variation in temporal SAV biomass changes estimated daily from water level slope. Light-colored bands are 95% confidence intervals, but are not always visible given their small sizes. For each year, a date of formal biomass measurement allowed for estimated SAV biomass to be validated (black points). Slopes are the trend extracted using EEMD from raw surface water elevation, which corresponded to the SAV flow obstruction effect. SAV submerged aquatic vegetation, LSP Lac Saint-Pierre. Lines are color-coded by water temperature using a warm to cold color gradient.

3.2 NO_3^- Budget

To estimate the NO_3^- budget for the plume flowing across the SAV meadow (Figure 1), we first compared the modelled NO_3^- input to the output of the in situ sensor measurements over five summers (Figure 4). The time series for the sensor were complete for 2012 and 2015 (88 and 93 days) and truncated by about 29 days for the other years due to instrument failure, with 2014 having the shortest time series (24 days). The comparison revealed that the NO_3^- output followed the same temporal pattern as the estimated inputs from the tributaries, but at markedly lower concentrations, regardless of the contribution of each tributary to NO_3^- inputs.

The contribution of each tributary to the incoming NO_3^- loads, estimated from conductivity, varied among years. Over the hot summers of 2012 and 2016, NO_3^- inputs

originated solely from Saint-François River, whereas over the remaining years (2013-2015), both rivers contributed approximately equally. We also observed that the daily NO_3^- concentration range measured at the outflow, which reflected daily retention by autotrophic assimilation, was most often considerably below estimated inputs, suggesting substantial removal by denitrification. The sensor occasionally exhibited abrupt changes and elevated daily concentrations, sometimes above estimated inputs, particularly in years when the Yamaska was contributing to the inputs. These changes coincided with both high NO_3^- concentrations from the Yamaska River combined with short-term high discharge events that increased its proportion to the total water inputs (SI Figure S5). We thus evaluated that on those days, tributary contributions to the outflowing water mass were poorly estimated. As such, we excluded these dates from budgets ($n_{excluded} = 31$, $n_{budget} = 292$) and assumed that the remaining NO_3^- inputs were accurately estimated.

The NO_3^- budget in the plume flowing across the SAV meadow also displayed high interannual variability (MANOVA $p < 0.001$) similar to the observed variation in temporal SAV biomass, and NO_3^- inputs and outputs for the complete SAV meadow (Figure 5). All variables contributed to among-year differences in budgets (LDA SI Table S3 and for process-specific rates and velocities $p < 0.03$). Using PCA, we observed that the uptake rates (particularly for U_t, U_a and U_d) were highly correlated to NO_3^- concentrations and tributary discharge ($r > 0.53$, Figure 5a). Variables describing proportional uptake (R and U_d/U_t) and V_f, both total and process-specific, where orthogonal to the uptake rates and were related to temperature and SAV abundance, both of which were markedly higher in August 2016 (up to day 228 of the year, last observation that year). In contrast, overall uptake rates tended to be differentiated by more generalized annual conditions where hotter and lower water levels years resulted in lower NO_3^- inputs and total retention than colder, higher water level years.

As such, this pattern of higher uptake measured in the plume was explained by the high NO_3^- loads in the colder years where both discharge and NO_3^- concentrations from tributaries (inputs) increased simultaneously ($r = 0.82$) and were strongly correlated to U_t ($r_{NO3} = 0.95$, $r_Q = 0.84$). Interannual variations in NO_3^- loads entering the meadow induced sharp differences in measured areal total uptake rates among years with median differences of up to 1.6 g m^{-2} d^{-1} (range: $med_{2012} = 0.1$ g m^{-2} d^{-1}, $med_{2014} = 1.7$ g m^{-2} d^{-1}, Figure 5b). Similarly to total NO_3^- inputs to the overall SAV meadow (Figure 2), high inflowing NO_3^- concentrations from the tributary

plume reflected the greater contribution of the heavily enriched and flashy Yamaska River waters. Inflowing NO_3^- concentrations to the plume were generally similar to those for the complete SAV meadow (Figure 2), except for 2013 and 2014 (Figure 5c). These discrepancies were due to the shortened periods when sensor data were available those years, with midsummer 2013 and early June 2014 having lower and higher NO_3^- inputs, respectively, than the rest of the summer (Figure 4). Both U_a and U_d followed a somewhat similar pattern as NO_3^- inputs (SI Figure S6), but 2013 displayed a distinctive pattern of high U_a as compared to its low inputs in NO_3^-. This is in part explained by lower U_d values, likely resulting from higher discharge and lower plant biomass. Apart from that year, U_d tended to be higher and had a wider range than U_a, reaching its maximum at 2.6 g m^{-2} d^{-1} (in 2015) compared to the maximum U_a of 1.9 g m^{-2} d^{-1} (in 2014).

In contrast to uptake rates, R was highest during hotter summers with a median increase of 5 to 27% as compared to colder years (med_{hot} = 69 to 82 %, med_{cold} = 55 to 64 %, Figure 5d). The low R measured over the two hottest years (2012 and 2016) could be explained by the up to three-fold reduction in discharge in comparison with colder years ($med_{2012,2016}$ = 36-69 m^3 s^{-1}, $med_{2013,\ 2014}$ = 78-100 m^3 s^{-1}). The low tributary discharge in 2012 and 2016 also nearly doubled water residence time in the plume ($med_{2012,\ 2016}$ = 50-60 h) compared to other summers ($med_{2013\text{-}2015}$ = 35-38 h, Figure S6). However, in 2015 the residence time and discharge were similar to the colder summers (med_{2015} = 35h, $med_{2013,\ 2014}$ = 35-38 h). In this case, the high R could be attributed to the higher SAV biomass of that year compared to colder ones; this factor likely also contributed to the high R in 2016. The higher total V_f ($V_{f\text{-}t}$) in the high biomass years (2015, 2016) also suggested that the increased biotic activity resulted in higher overall retention and uptake rates (Figure 5e-g). Additionally, the summers of 2015 and 2016 tended to have proportion of denitrification from total uptake (U_d/U_t) 11 to 37 % higher than others, suggesting an interplay between climate and SAV biomass on N fate (SI Figure S6). To further investigate whether the changing SAV biomass affected the partitioning of N retention pathways, we compared yearly medians of process-specific ($V_{f\text{-}a}$, $V_{f\text{-}d}$) to total uptake velocity ($V_{f\text{-}t}$, Figure 6). The higher $V_{f\text{-}t}$ in the high biomass years could be attributed to either generally higher uptake velocity due to denitrification ($V_{f\text{-}d}$, in 2015) or higher daily values that increased variation around the estimate (2016). By comparison, when SAV biomass was reduced, $V_{f\text{-}d}$ was lower (2013) or similar (2012, 2014) to uptake velocity due to autotrophic assimilation ($V_{f\text{-}a}$).

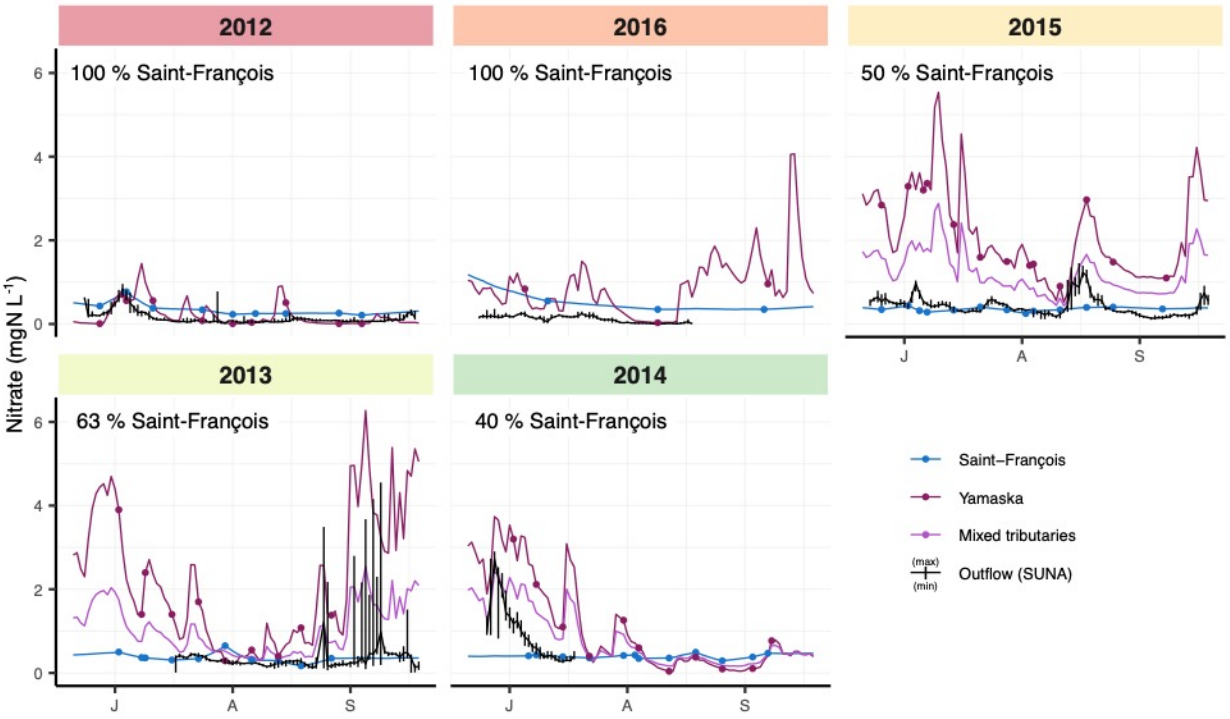

Figure 4. Daily NO_3^- inputs from individual tributaries as well as their estimated mixing concentrations in the plume compared to the median NO_3^- measured at the SAV bed outflow by the in situ sensor. Black vertical bars represent daily minimum and maximum NO_3^- concentration at the outflow. For tributaries, lines are fitted concentration values from the loadflex composite approach and points are measurements. Estimated input contributions from the Saint-François River are indicated on each panel with the remaining proportion coming from the Yamaska River. Mixed tributary lines for 2012 and 2016 are not presented since estimated inputs are solely from the Saint-François River. Panels are ordered by summer water temperature and water level (from hot-low level on top to cold-high on the bottom).

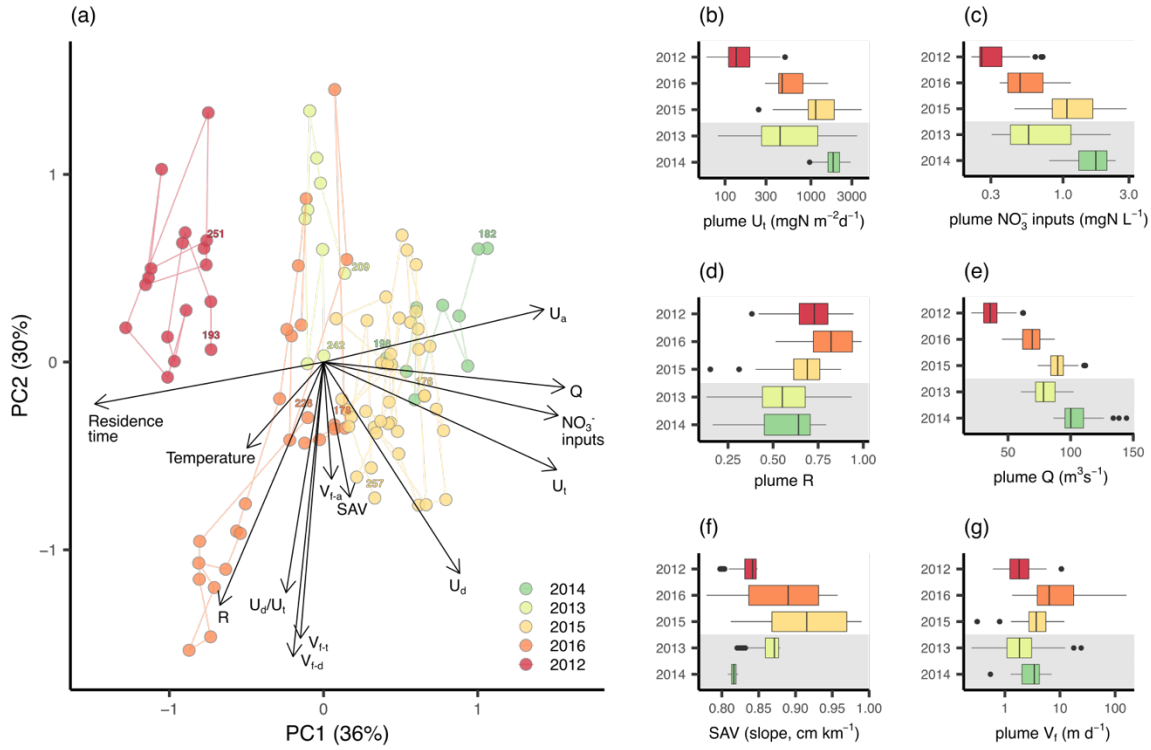

Figure 5. Correlative relationships and interannual variation in NO_3^- budget terms and their potential predictors in the plume flowing across the SAV meadow. A) principal component analysis (PCA) using scaling 2 where angles between arrows approximate correlation between variables. B) to G) show interannual distributions with vertical bars within boxes indicating median value, box boundaries representing 25th and 75th percentile and whiskers ranging from 10th to 90th percentiles. PC principal components with explained variance in parentheses, U uptake rate, R proportion of NO_3^- retained, Q discharge, SAV submerged aquatic vegetation, V_f uptake velocity, $_t$ total, $_a$ autotrophic assimilation, $_d$ denitrification. In a), colored numbers correspond to the first and last day of the year of estimation, and lines connect observations in temporal order. Years are ordered by decreasing water temperature using a warm to cold color gradient; cold summers are indicated by light grey shaded background.

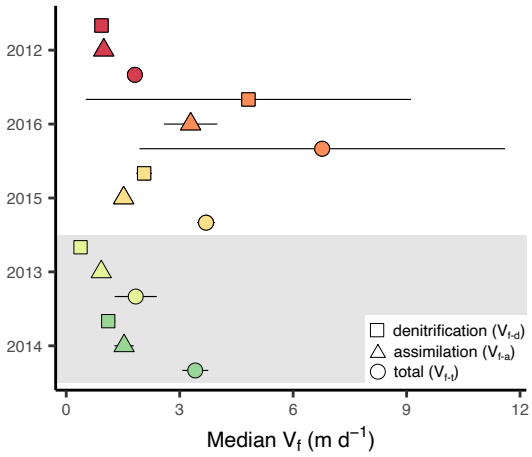

Figure 6. Comparison of median uptake velocity (V_f) from denitrification and autotrophic assimilation to total uptake velocity per summer. Error bars are standard error. Years are ordered by decreasing water temperature using a warm to cold color gradient; cold summers are indicated by the light grey shaded background.

3.3 Prediction of Total NO_3^- Retention by the SAV Meadow

To estimate summertime NO_3^- retention in the complete SAV meadow, we built regression models using our NO_3^- budget in the plume and its relationship with environmental variables. The model to predict U_t with the highest AIC included both NO_3^- inputs and the temporal SAV biomass estimate (SI Table S4) but, this model was not selected because the AIC improvement was minor (< 2) compared to the simplest model with only one predictor. Given the strong relationship between retention and inputs, U_t could be predicted solely from NO_3^- concentration of those inputs (marginal $R^2 = 0.88$, SI Table S5). The intercepts of the NO_3^- and U_t relationship differed among years (conditional $R^2 = 0.92$). Although the AIC difference was minor with the model without random structure, variable intercept per year was selected because it homogenized the residual variance among years (SI, Table S6). Most importantly, the model was substantially improved by adding an autocorrelation structure per date (autoregressive model, AR-1), which considers that consecutive observations were highly correlated with each other ($r = 0.82$). Using the fixed effect of the model with only NO_3^- as a predictor (SI Table S5) and weighted concentrations of tributaries derived from the plume, we predicted U_t for the

595 complete SAV bed and summer period and derived R from yearly NO_3^- load (Table 2). Retention
596 was highly variable among years, showing a fourfold difference between extremes. The
597 interannual pattern in retention was similar to patterns in inputs, albeit the inputs exhibited a
598 much higher interannual variation than the outputs, with almost a sixfold difference between
599 extreme N loads. As a result, R tended to be somewhat higher (63-87%) in the warmer years
600 (2012, 2016, 2015) than in colder years (47-62%). A nearly complete retention (87%) was
601 observed in 2016, concomitant with lower NO_3^- inputs. When calculating U_d from the overall
602 SAV bed U_t using the median plume U_d/U_t, these differences in retention with climate were more
603 important. Year with higher SAV biomass or lower NO_3^- inputs had 30 to 58% of inputs
604 permanently removed through denitrification compared to 18-22% during colder years with
605 reduced SAV biomass and higher NO_3^- loads.

606 **Table 2.** Whole-SAV meadow summertime NO_3^- inputs, total and denitrification uptake (U_t, U_d),
607 and proportional retention (R) modelled for six summers (June 21 to September 22). Nitrate
608 inputs were estimated from the sum of daily tributary loads. U_t was modelled from daily inputs,
609 using NO_3^- concentrations as the predictive variable, while U_d was estimated by multiplying U_t
610 by the plume yearly median proportion of U_d on U_t. Maximum SAV biomass was estimated from
611 the linear regression between rake estimated biomass and water level slope. CI confidence
612 intervals, denit. denitrification. Summers are ordered by decreasing water temperature.

Year	**Total NO_3^- inputs** (tonnes)	**U_t** (tonnes)	**U_t 95% CI** (tonnes)	**U_d** (tonnes)	**R total** (%)	**R denit.** (%)	**Maximum SAV biomass** (g m^{-2})
2012	304	192	[173, 214]	91	63	30	31
2016	533	466	[392, 555]	311	87	58	109
2015	1188	751	[610, 927]	441	63	37	127
2013	1811	846	[670, 1073]	250	47	14	52
2014	726	444	[373, 529]	158	61	22	20
2017	622	384	[329, 448]	113	62	18	50

613

4 Discussion

In this study, we provide high frequency measures of N retention and its partitioning into autotrophic and heterotrophic pathways across multiple years from a riverine SAV meadow, in one of the largest rivers to date. We hypothesized that retention, measured as either uptake rates (U) and proportion retained from inputs (R), would be a function of NO_3^- loads and of vegetation biomass, both of which expected to be subject to climate-driven variations. We found that N retention by the meadow in the main stem significantly attenuated the incoming loads from two enriched agriculturally impacted tributaries. Estimated rates were among the highest reported so far in rivers (U_t median 576 mg N m^{-2} d^{-1}, range 60 – 3893 mg N m^{-2} d^{-1}), showing both annual and interannual variations of this ecosystem service as a function of climate conditions. This variation highlights the importance of measuring N retention rates multiple times within a year and across several years. NO_3^- uptake rates in the SAV meadow were a function of NO_3^- loads, which varied largely as a function of climate driven changes in discharge from the tributaries. However, the climate effect on loads were not in synchrony with the water level changes in the main stem. This was probably due to differential effect of precipitation patterns on basin-wide water inputs and aspects related to regulated flow upstream from the study site versus localized water inputs at the confluence. Proportional retention was higher in the hottest years and coincided with either higher water residence time or higher SAV biomass in the meadow or both. Maximum summer SAV biomass appeared to vary along a dome-shaped curve, and optimal conditions were observed in summers with warm water temperatures, average water levels, and loadings of abundant NO_3. Higher SAV biomass also influenced the partitioning of N retention pathways by promoting permanent removal through higher denitrification. Our work indicates that this riverine SAV meadow provides an important ecosystem service by reducing N export to downstream waters by 47 to 87% and permanently removing between 14 and 58% of N inputs. Thus, management actions should aim at preserving or restoring such critical riverine N removal control points.

4.1 Nitrogen Retention in Riverine SAV Meadows

Vegetated sites in rivers are recognized for performing multiple aquatic ecosystem services including N removal (Caraco et al., 2006). However, measuring seasonal and interannual changes in SAV biomass and how it affects N processing in large meadows remains

a challenge due to the restricted ability to assess biomass changes underwater and the difficulty to measure N retention in large river. We successfully followed SAV biomass daily using the indirect measure of water level slope and N retention using a high frequency sensor. Using this information, we found that only part of our hypothesis was supported as there was no conclusive evidence of a strong relationship between uptake rates and SAV biomass. This was likely due to the overriding role of NO_3^- inputs in determining total uptake rates (U_t) of the meadow. The strong relationship between inputs and U_t is not suprising as N retention is typically modelled using first-order kinetics, where process rates are a linear (log-log) function of substrate concentrations (e.g. Seitzinger et al., 2006; Wollheim et al., 2006). For a maximal functioning, N removal sites thus have to be spatially connected to high N loading locations, as is the case for the confluence zone of this study (Cheng et al., 2020; Mitsch et al., 2001).

The strong positive effect of SAV biomass on N uptake rates has previously been reported when comparing river reaches with contrasting plant cover (85% vs 45%, SI Table S7, Preiner et al., 2020). We did not observe a clear pattern with plant biomass probably because SAV cover was always high across the N budget plume, thus always favoring high N uptake. Rather, the interannual differences in SAV was one of plant density, or biomass, which likely changed SAV surface area as these two measures of SAV are well correlated (Armstrong et al., 2003). Greater SAV surface area obstructs flow, which reduces velocity and increases water residence time (Madsen et al., 2001). This latter increase should also increase the proportion of N retained since a prolonged contact between water column NO_3^- with plants and sediments can lead to the exhaustion of this substrate pool. Indeed, and as typically observed (Seitzinger et al., 2006), there was a general inversed interannual pattern between proportion retained and discharge (Figure 5d-e). However, high biomass years (2015, 2016) had higher than expected retention (1st and 3rd highest) given their fast flow and high discharge (4nd and 2nd highest). Higher biomass years therefore probably had added plant surface area facilitating N exchange between plants, their epiphytes, sediments, and water column.

Additionally, our results suggest that changing SAV biomass affected N fate. When SAV was abundant, denitrification rates in the plume were high and accounted for 59 to 67% of total uptake in contrast to 30 to 48% during years when biomass was reduced. Similarly, when using V_f, a metric that is independent of concentrations and hydrologic characteristics (Ensign & Doyle, 2006; Wollheim et al., 2006), the biotic demand of denitrification ($V_{f\text{-}d}$) was higher than

675 that of assimilation during high biomass years, and vice versa. At the scale of the SAV bed, these
676 differences translated into an up to four times higher rate of permanent removal in high biomass
677 years compared to lower ones. These results are in agreement with studies that considered both
678 assimilatory and dissimilatory pathways (Heffernan & Cohen, 2010; James, 2010; Pinardi et al.,
679 2009; Preiner et al., 2020, summarized in SI Table S7), while reports focusing solely on N
680 assimilation by SAV and their epiphytes generally found that overall uptake of water column
681 NO_3^- concentrations were typically lower (Desmet et al., 2011; Diamond et al., 2021). The
682 dominance of denitrification in a higher biomass year can be explained by the structural
683 complexity of SAV and increased surface area that supports biofilms where denitrification can
684 occur (Eriksson & Weisner, 1996). SAV also favors denitrification in sediments, by promoting
685 organic matter particle settling, which increases sediment respiration rates and the anoxic
686 conditions needed for denitrification (Cornwell etal. 1999). Furthermore, SAV provide labile
687 dissolved organic matter directly to denitrifiers within the sediments through the release of
688 exudates from their roots (Karjalainen et al., 2001). Overall, in advection-dominated systems
689 such as rivers where NO_3^- is continuously supplied from the watershed (Seitzinger et al., 2006),
690 the dominance of denitrification on total uptake in SAV beds is likely a function of how plants
691 amplify reactive surface areas, enrich sediments, and increase contact rates through a reduction
692 in flow creating optimal environmental conditions for denitrifying microbes.

693 Given the optimal conditions for N processing at our SAV control point, both total N
694 uptake and denitrification rates measured in this study (U_t = 576 [60-3893 mg N m^{-2} d^{-1}] ,U_d =
695 338 mg N m^{-2} d^{-1} [1-2624 mg N m^{-2} d^{-1}] SI Table S7) are among the highest reported, but remain
696 within the range of previous estimates derived from similar methods in SAV meadows [up to
697 840 mg Nm^{-2} d^{-1}], Heffernan & Cohen, 2010; Preiner et al., 2020). Our estimates are also higher
698 than those previously reported in a meta-analysis of denitrification in rivers worldwide (up to
699 1143 mg m^{-2} d^{-1}, Piña-Ochoa & Álvarez-Cobelas, 2006). This may be due to differences across
700 methods, temporal and spatial scales of inquiry, and the presence, size and location of the SAV
701 bed under study. The meta-analysis involved short-term laboratory (cores) or in situ (chambers)
702 incubations providing discrete denitrification rates in time. We report daily and interannual net
703 uptake rates at the reach-scale that reflect the balance between processes that produce
704 (nitrification) and consume NO_3^- (assimilation, denitrification), and its variability throughout
705 multiple growing seasons. Our estimates may be higher because of a greater sensitivity of the

two-station mass-balance approach to increase in NO_3^- concentration and reach length (von Schiller et al., 2011). Still, the uptake rates from this method are generally in agreement with multiple site mass-balance and incubation approaches (Piña-Ochoa & Álvarez-Cobelas, 2006; von Schiller et al., 2011). The importance of the size and location of vegetated areas on flow modification and N attenuation is highlighted by the similar denitrification rates measured in a dense floating bed of *Trapa natans* in a sheltered bay of the Hudson River (1.5 km^2, 518-994 mg N m^{-2} d^{-1}), in contrast to the undetectable rates in a small (0.6 km^2) *Vallisneria* meadow in a fast-flowing channel from the same river (Tall et al., 2011). The floating meadow acted in a similar way to this study large SAV meadow (~10 km^2) that both intercepted nutrient-rich waters and reduced velocities (Bulat et al., 2019), thus promoting high nitrate removal. Another line of evidence supporting the robustness of our estimates is that our measured uptake velocities (V_f, median 3.0 m d^{-1}) were similar to those reported for the Upper Snake River (WY, USA, 12 m^3 s^{-1}, 0.6 to 13.0 m d^{-1}, Tank et al., 2008). However, our estimates were much more variable both within and among seasons (range 0.2 – 160.8 m d^{-1}), highlighting the considerable heterogeneity of biotic activity, load and NO_3^- retention capacity in time at this dynamic confluence zone.

4.2 Complex Effects of Climate at a Confluence Zone

By measuring environmental conditions over 6 summers, we showed that different climatic variables drove complex variations in SAV biomass and N retention in a large riverine SAV meadow. The predominant influence of climate on SAV biomass was perceptible through the large range of water levels and temperatures among years: our observations spanned the lowest (2012) and highest (2017) mean summer water levels recorded at LSP gauging station for more than a century (data available since 1914, meds-sdmm.dfo-mpo.gc.ca). Our observations also included the warmest (2012) and the third coolest (2014) mean summer water temperature over the last 20 years (data available since 2000, ogsl.ca). These climatic variations translated into a ≈6-fold range in maximum SAV biomass within the study area during the 2012-2017 period (Table 2).

The range in climate variation captured on such a short time scale reflect the sensitivity of rivers to these changes and impacts that are likely already taking place (Gudmundsson et al., 2021; Nijssen et al., 2001). Among these impacts, we could expect that increased precipitation should favor N transport, as is generally seen in anthropogenically altered river networks

(Goyette et al., 2019; Howarth et al., 2012). Inflowing NO_3^- concentrations to the SAV meadow were correlated to the discharge of incoming tributaries, but concentrations changes were mostly a function the relative contribution of each tributary to the total at the confluence site, particularly from the smaller, more NO_3^- rich, and flashier Yamaska River. This river displayed the typical seasonality of agricultural watershed where discharge and NO_3^- concentrations vary in synchrony (Van Meter et al., 2020). Indeed, in smaller catchments like the Yamaska, riverine nutrient loads are typically more variable than in larger catchments, like the Saint-François (2.1 times larger than Yamaska) and the SLR main stem, which integrate loads from many sub-watersheds that dampens individual basin signals (Burt & Pinay, 2005; Chezik et al., 2017). However, the variation in NO_3^- inputs was disconnected from temperature and water level variation in the main stem that was more reflective of water inputs at the scale of the entire SLR watershed. These asynchronies might become more common as more pronounced climate-driven changes and reduced summer discharge are expected over the next decade in southern SLR tributaries, in contrast to maintained or amplified discharge in northern SLR tributaries (Boyer et al., 2010; Ouranos, 2015). Regardless, the highest SAV biomass were recorded at the confluence zone over years of intermediate water level and temperature conditions.

Past observations suggest that optimal conditions for SAV biomass are met when water levels are high in LSP, and are limited when levels are low, favoring reed bed expansion (Hudon, 1997). We observed the latter in the extremely low-level year of 2012. SAV biomass was among the lowest recorded during this study and can be explained by the large areas of riverbed being exposed to air that year, potentially leading to SAV loss through the dry-out of above ground biomass. The elevated water temperatures might also have favored phytoplankton and metaphyton growth that year through slow water transit time, high water column illumination and increased nutrient release from the sediments. Indeed, low water levels in LSP are associated with increased filamentous green algae biomass (Cattaneo et al., 2013). Overall highest TP (~39 $\mu g\ L^{-1}$), chlorophyll *a* (~3.6 $mg\ L^{-1}$) and lowest secchi depths (~67 cm) were also measured within the bed in 2012 despite average TP inputs (Figure 2g). In contrast with Hudon (1997), however, our result suggests that SAV biomass is also constrained at extremely high water level years when temperatures are cold. The effect of high waters can be explained by SAV light limitations through the typical positive relationship between maximum SAV colonization depth and water transparency (e.g. Chambers & Kalff, 1985). Incoming turbidity did not display a

767 coherent pattern as a function of water level changes (Figure S4), and increased water height in
768 itself likely created deep areas where light did not reach the bottom, thus restricting plant
769 colonization. In the LSP fluvial lake, the deeper waters also correspond to an increased exposure
770 to fast currents, further limiting SAV growth (Hudon et al., 2000).

771 When water depth and transparency allowed light penetration to the sediments and thus
772 plants were not limited by light, increases in temperature probably directly favored SAV growth
773 and biomass accumulation. This has previously been shown in nearby shallow lakes where sharp
774 differences in SAV biomass for the same lakes were observed in a cold and a hot year (Rooney
775 & Kalff, 2000). The direct effect of temperature is likely a function of increased photosynthetic
776 rates that drive plant growth (Brown et al., 2004; Farquhar et al., 1980; Riis et al., 2012).
777 Experimental studies support this potential direct effect in mesotrophic conditions, when light
778 availability does not limit plant growth (Barko et al., 1982; Ersoy et al., 2020). These conditions
779 were met in intermediate water level and hotter years (2015-2016) where TP within the meadow
780 ranged from ~19-26 µg P L^{-1}. During those years, SLR temperature was near the previously
781 determined growth optimum of ~25-28ºC, below deleterious temperatures (28-30 °C, Barko et
782 al., 1982; Riis et al., 2012). Indeed, during our field survey, water temperatures were always
783 below 27.2 °C and generally around 24 °C during 2015 and 2016. The intermediate water level
784 of those years likely also increased light availability to a more extensive area for SAV growth
785 (Beklioglu & Altinayar, 2006). SAV growth during those years might also have been facilitated
786 by the time lag that allowed for plant bed recovery following the 2012 drawdown that potentially
787 damaged winter buds and reduced biomass the subsequent years. We argue that this is unlikely
788 as SAV bed can regenerate from seed banks (Kimber et al., 1995), and the 2012 event still left
789 large meadow areas covered with water. Additionally, the highest biomass year (2016) was
790 followed by a low biomass year, suggesting that autocorrelation between consecutive years was
791 not a dominant driver of SAV biomass during our study period. Our results rather indicate that
792 water levels combined with water temperature seems critical in determining biomass as for
793 example in 2014 when water levels were similar to the high biomass year of 2015 and 2016,
794 temperatures were coldest and SAV biomass was lowest. As such, when areal light to sediment
795 is apparently equal, temperatures in hot years directly stimulated SAV growth in LSP.

5 Conclusions

In this study, we showed the complex influence of climate on N retention in a SAV meadow in the SLR and report some of the highest measured estimates in a large river from this control point. This influence includes modulating N loads to the meadow combined with SAV biomass and water residence time within it, mitigating the total amount and the proportion of N retained, as well as N fate. Our results suggest that SAV biomass is restricted by extreme dry and wet years, which may increase in frequency with climate change, thus suggesting a diminishing role of SAV on N retention in the SLR. Indeed, SLR water levels have been decreasing since the 1970s (Hudon et al., 2018), and climate projections of increasing summer air temperatures will further reduce levels through higher evaporative loss. However, higher precipitations are projected with climate change, particularly in the North (Ouranos, 2015), which might also lead to more floods as observed in 2017 and sustained high water levels throughout summers. There was no direct correlation between SLR water levels and tributary NO_3^- loads at our confluence site, probably due to asynchronous precipitation patterns across sub-watersheds in the SLR basin. During years with overall higher tributary discharge, short-term, heavy precipitation patterns favored the flashiness of the Yamaska River, yielding high inflow of turbid, nutrient-rich waters. Our sensor time series displayed more frequent NO_3^- spikes following summer rain, potentially reflecting higher N export during these events due to reduced water residence time. As extreme precipitation events are expected to become more common with climate change, these moments might increasingly contribute to N exports (Goyette et al., 2019; Lu et al., 2020). However, we could not calculate N budgets during these events because of the changing tributary contribution to waters flowing through the SAV meadow. Future studies should investigate how such events contribute to overall N exports and assess whether SAV lose their capacity to dampen hydraulic flows and retain N under such circumstances.

Although wetlands in watersheds are considered to have a disproportionate role in N retention on the landscape (Cheng et al., 2020), we argue that shallow-water underwater plant meadows should also be considered in conservation assessments. Even when SAV biomass was low, the meadow provided an important ecosystem service by retaining large amounts of N, thus decreasing impacts of overall N delivery from agricultural rivers to the SLR estuary. The proportion retained and permanently removed was highest during hotter years with high SAV biomass, while the absolute amount retained was related to N loads which reflected localized

827 precipitation patterns from the two tributary watersheds. Although the effect of SAV is seasonal,
828 it coincides with the period when N export has the highest potential impact in the SLR estuary by
829 contributing to the reported eutrophication, which partially explains growing hypoxia in its deep
830 waters (Gilbert et al., 2005; Lehmann et al., 2009). We estimate that during the SAV growing
831 season, between 2 to 9 t N per day could be retained, which is higher than previous estimates of
832 1.5 t N per day from this same location using a coarser mass-balance approach (Hudon et al.,
833 2017). Assuming a 1.1 kg N per summer based on an annual per capita excretion of 4.4 kg N yr^{-1}
834 (Howarth et al., 1996), this would be the equivalent of retaining the N generated by a city of 0.17
835 to 0.77 million people over the SAV growing season. Although we illustrated the value of SAV
836 meadows from a N perspective, other cultural and provisioning services are supplied by SAV in
837 general (Hilt et al., 2017) and in particular at our site, commercial and recreational fisheries
838 (Giacomazzo et al., 2020; He et al., 2016). Therefore, management action should aim at
839 preserving or restoring such critical sites within the shallow-water areas of large rivers.

840 **Acknowledgments**

841 We thank the numerous people that provided assistance for sample and biomass
842 collection and subsequent lab analyses throughout the years, Jean-Pierre Amyot and Conrad
843 Beauvais for installation and maintenance of the SUNA, as well as Nicolas Fortin St-Gelais,
844 Richard Labrie and Pierre Gagnon for advice on data analyses. This project was funded by the
845 Groupe de recherche interuniversitaire en limnologie (GRIL) through a Fonds de recherche de
846 Québec - Nature et technologies (FRQNT) Initiatives stratégiques pour l'innovation grant,
847 National Sciences and Engineering Research Council of Canada (NSERC) Discovery to RM, and
848 FRQNT and NSERC scholarships to MB. This work was also supported by Environment and
849 Climate Change Canada (ECCC) as part of the Canada-Québec St. Lawrence Action Plan
850 (SPLAP, CH). We acknowledge that this work was carried out on the traditional lands stewarded
851 by the N'dakina (Abenaki / Abénaquis).

852 **Open Research**

853 Data used for figure creation and statistical analysis in this study are all openly available
854 at the Zenodo repository via https://doi.org/10.5281/zenodo.6413187 with license under a
855 Creative Commons Attribution 4.0 International.

References

Alexander, R. B., Smith, R. A., & Schwarz, G. E. (2000). Effect of stream channel size on the delivery of nitrogen to the Gulf of Mexico. *Nature*, *403*(6771), 758-761. https://doi.org/10.1038/35001562

Appling, A. P., Leon, M. C., & McDowell, W. H. (2015). Reducing bias and quantifying uncertainty in watershed flux estimates: the R package loadflex. *Ecosphere*, *6*(12), 1-25. https://doi.org/https://doi.org/10.1890/ES14-00517.1

Armstrong, N., Planas, D., & Prepas, E. (2003). Potential for estimating macrophyte surface area from biomass. *Aquatic Botany*, *75*(2), 173-179, Article Pii s0304-3770(02)00169-9. https://doi.org/10.1016/s0304-3770(02)00169-9

Audet, J., Olsen, T. M., Elsborg, T., Baattrup-Pedersen, A., & Riis, T. (2021). Influence of plant habitats on denitrification in lowland agricultural streams. *Journal of Environmental Management*, *286*, Article 112193. https://doi.org/10.1016/j.jenvman.2021.112193

Ballard, T. C., Sinha, E., & Michalak, A. M. (2019). Long-Term Changes in Precipitation and Temperature Have Already Impacted Nitrogen Loading. *Environmental Science & Technology*, *53*(9), 5080-5090. https://doi.org/10.1021/acs.est.8b06898

Barko, J. W., Hardin, D. G., & Matthews, M. S. (1982). Growth and morphology of submersed freshwater macrophytes in relation to light and temperature. *Canadian Journal of Botany*, *60*(6), 877-887.

Bekka, R. E. H., & Berrouche, Y. (2013). Improvement of ensemble empirical mode decomposition by over-sampling. *Advances in Adaptive Data Analysis*, *05*(03), 1350012. https://doi.org/10.1142/s179353691350012x

Beklioglu, M., & Altinayar, G. T. (2006). Water level control over submerged macrophyte development in five shallow lakes of Mediterranean Turkey. *Archiv für Hydrobiologie*, 535-556.

Benda, L., Poff, N. L., Miller, D., Dunne, T., Reeves, G., Pess, G., & Pollock, M. (2004). The Network Dynamics Hypothesis: How Channel Networks Structure Riverine Habitats. *BioScience*, *54*(5), 413-427. https://doi.org/10.1641/0006-3568(2004)054[0413:Tndhhc]2.0.Co;2

Bernhardt, E. S., Blaszczak, J. R., Ficken, C. D., Fork, M. L., Kaiser, K. E., & Seybold, E. C. (2017). Control Points in Ecosystems: Moving Beyond the Hot Spot Hot Moment Concept. *Ecosystems*, *20*(4), 665-682. https://doi.org/10.1007/s10021-016-0103-y

Botrel, M., Hudon, C., Biron, P. P., & Maranger, R. (2022). Combining quadrat, rake and echosounding to estimate submerged aquatic vegetation biomass at the ecosystem scale. *bioRxiv*, https://doi.org/10.1101/2022.03.15.484486

Boudreau, P. A., Leclerc, M., & Fortin, G. (1994). Modélisation hydrodynamique du lac Saint-Pierre, fleuve Saint-Laurent : l'influence de la végétation aquatique. *Canadian Journal of Civil Engineering*, *21*, 471-489.

Bowman, D. C., & Lees, J. M. (2013). The Hilbert–Huang Transform: A High Resolution Spectral Method for Nonlinear and Nonstationary Time Series. *Seismological Research Letters*, *84*(6), 1074-1080. https://doi.org/10.1785/0220130025

Boyer, C., Chaumont, D., Chartier, I., & Roy, A. G. (2010). Impact of climate change on the hydrology of St. Lawrence tributaries. *Journal of Hydrology*, *384*(1–2), 65-83. https://doi.org/http://doi.org/10.1016/j.jhydrol.2010.01.011

Britton, C. M., & Dodd, J. D. (1976). Relationships of photosynthetically active radiation and shortwave irradiance. *Agricultural Meteorology*, *17*(1), 1-7. https://doi.org/https://doi.org/10.1016/0002-1571(76)90080-7

Brown, J. H., Gillooly, J. F., Allen, A. P., Savage, V. M., & West, G. B. (2004). Towart a metabolic theory of ecology. *Ecology*, *85*(7), 1771-1789. https://doi.org/https://doi.org/10.1890/03-9000

Bulat, M., Biron, P. M., Lacey, J. R. W., Botrel, M., Hudon, C., & Maranger, R. (2019). A three-dimensional numerical model investigation of the impact of submerged macrophytes on flow dynamics in a large fluvial lake. *Freshwater Biology*, *64*(9), 1627-1642. https://doi.org/10.1111/fwb.13359

Burt, T. P., & Pinay, G. (2005). Linking hydrology and biogeochemistry in complex landscapes. *Progress in Physical Geography: Earth and Environment*, *29*(3), 297-316. https://doi.org/10.1191/0309133305pp450ra

912 Caraco, N., Cole, J., Findlay, S., & Wigand, C. (2006). Vascular Plants as Engineers of
913 Oxygen in Aquatic Systems. *BioScience*, *56*(3), 219-225. https://doi.org/10.1641/0006-
914 3568(2006)056[0219:Vpaeoo]2.0.Co;2

915 Caraco, N. F., & Cole, J. J. (1999). Human impact on nitrate export: an analysis using
916 major world rivers. *Ambio*, *28*(2), 167-170.

917 Carpenter, S. R., Caraco, N. F., Correll, D. L., Howarth, R. W., Sharpley, A. N., & Smith,
918 V. H. (1998). Nonpoint pollution of surface waters with phosphorus and nitrogen. *Ecological*
919 *Applications*, *8*(3), 559-568. https://doi.org/https://doi.org/10.1890/1051-
920 0761(1998)008[0559:NPOSWW]2.0.CO;2

921 Cattaneo, A., Hudon, C., Vis, C., & Gagnon, P. (2013). Hydrological control of
922 filamentous green algae in a large fluvial lake (Lake Saint-Pierre, St. Lawrence River, Canada).
923 *Journal of Great Lakes Research*, *39*(3), 409-419.
924 https://doi.org/http://dx.doi.org/10.1016/j.jglr.2013.06.005

925 Chamberlin, C. A., Katul, G. G., & Heffernan, J. B. (2021). A Multiscale Approach to
926 Timescale Analysis: Isolating Diel Signals from Solute Concentration Time Series.
927 *Environmental Science & Technology*, *55*(18), 12731-12738.
928 https://doi.org/10.1021/acs.est.1c00498

929 Chambers, P. A., & Kalff, J. (1985). Depth distribution and biomass of submersed
930 aquatic macrophyte communities in relation to Secchi depth. *Canadian Journal of Fisheries and*
931 *Aquatic Sciences*, *42*(4), 701-709.

932 Cheng, F. Y., Van Meter, K. J., Byrnes, D. K., & Basu, N. B. (2020). Maximizing US
933 nitrate removal through wetland protection and restoration. *Nature*, *588*(7839), 625-630.
934 https://doi.org/10.1038/s41586-020-03042-5

935 Chezik, K. A., Anderson, S. C., & Moore, J. W. (2017). River networks dampen long-
936 term hydrological signals of climate change. *Geophysical Research Letters*, *44*(14), 7256-7264.
937 https://doi.org/https://doi.org/10.1002/2017GL074376

938 Cole, J. J., & Caraco, N. F. (1998). Atmospheric exchange of carbon dioxide in a low-
939 wind oligotrophic lake measured by the addition of SF6. *Limnology and Oceanography*, *43*(4),
940 647-656. https://doi.org/https://doi.org/10.4319/lo.1998.43.4.0647

941 Desmet, N. J. S., Van Belleghem, S., Seuntjens, P., Bouma, T. J., Buis, K., & Meire, P.
942 (2011). Quantification of the impact of macrophytes on oxygen dynamics and nitrogen retention
943 in a vegetated lowland river. *Physics and Chemistry of the Earth*, *36*(12), 479-489.
944 https://doi.org/10.1016/j.pce.2008.06.002

945 Diamond, J. S., Moatar, F., Cohen, M. J., Poirel, A., Martinet, C., Maire, A., & Pinay, G.
946 (2021). Metabolic regime shifts and ecosystem state changes are decoupled in a large river.
947 *Limnology and Oceanography*, *n/a*(n/a). https://doi.org/https://doi.org/10.1002/lno.11789

948 Ensign, S. H., & Doyle, M. W. (2006). Nutrient spiraling in streams and river networks.
949 *Journal of Geophysical Research: Biogeosciences*, *111*(G4).
950 https://doi.org/https://doi.org/10.1029/2005JG000114

951 Eriksson, P., & Weisner, S. (1996). Functional differences in epiphytic microbial
952 communities in nutrient-rich freshwater ecosystems: an assay of denitrifying capacity.
953 *Freshwater Biology*, *36*(3), 555-562. https://doi.org/https://doi.org/10.1046/j.1365-
954 2427.1996.00120.x

955 Ersoy, Z., Scharfenberger, U., Baho, D. L., Bucak, T., Feldmann, T., Hejzlar, J., . . .
956 Beklioğlu, M. (2020). Impact of nutrients and water level changes on submerged macrophytes
957 along a temperature gradient: A pan-European mesocosm experiment. *Global Change Biology*,
958 *26*(12), 6831-6851. https://doi.org/https://doi.org/10.1111/gcb.15338

959 Ezer, T., & Corlett, W. B. (2012). Is sea level rise accelerating in the Chesapeake Bay? A
960 demonstration of a novel new approach for analyzing sea level data. *Geophysical Research*
961 *Letters*, *39*(19). https://doi.org/https://doi.org/10.1029/2012GL053435

962 Farquhar, G. D., von Caemmerer, S., & Berry, J. A. (1980). A biochemical model of
963 photosynthetic CO2 assimilation in leaves of C3 species. *Planta*, *149*(1), 78-90.
964 https://doi.org/10.1007/BF00386231

965 Galloway, J. N., Aber, J. D., Erisman, J. W., Seitzinger, S. P., Howarth, R. W., Cowling,
966 E. B., & Cosby, B. J. (2003). The Nitrogen Cascade. *BioScience*, *53*(4), 341-356.
967 https://doi.org/10.1641/0006-3568(2003)053[0341:Tnc]2.0.Co;2

968 Giacomazzo, M., Bertolo, A., Brodeur, P., Massicotte, P., Goyette, J.-O., & Magnan, P.
969 (2020). Linking fisheries to land use: How anthropogenic inputs from the watershed shape fish

habitat quality. *Science of The Total Environment*, *717*, 135377. https://doi.org/https://doi.org/10.1016/j.scitotenv.2019.135377

Gilbert, D., Sundby, B., Gobeil, C., Mucci, A., & Tremblay, G. H. (2005). A seventy-two-year record of diminishing deep-water oxygen in the St. Lawrence estuary: The northwest Atlantic connection. *Limnology and Oceanography*, *50*(5), 1654-1666.

Goyette, J.-O., Bennett, E. M., Howarth, R. W., & Maranger, R. (2016). Changes in anthropogenic nitrogen and phosphorus inputs to the St. Lawrence sub-basin over 110 years and impacts on riverine export. *Global Biogeochemical Cycles*, *30*(7), 1000-1014. https://doi.org/10.1002/2016gb005384

Goyette, J.-O., Bennett, E. M., & Maranger, R. (2019). Differential influence of landscape features and climate on nitrogen and phosphorus transport throughout the watershed. *Biogeochemistry*, *142*(1), 155-174.

Gudmundsson, L., Boulange, J., Do, H. X., Gosling, S. N., Grillakis, M. G., Koutroulis, A. G., . . . Papadimitriou, L. (2021). Globally observed trends in mean and extreme river flow attributed to climate change. *Science*, *371*(6534), 1159-1162.

Hall, R. O., Baker, M. A., Rosi-Marshall, E. J., Tank, J. L., & Newbold, J. D. (2013). Solute-specific scaling of inorganic nitrogen and phosphorus uptake in streams. *Biogeosciences*, *10*(11), 7323-7331. https://doi.org/10.5194/bg-10-7323-2013

Hall, R. O., & Tank, J. L. (2003). Ecosystem metabolism controls nitrogen uptake in streams in Grand Teton National Park, Wyoming. *Limnology and Oceanography*, *48*, 1120-1128.

Hall, R. O., Tank, J. L., Sobota, D. J., Mulholland, P. J., O'Brien, J. M., Dodds, W. K., . . . Arangob, C. P. (2009). Nitrate removal in stream ecosystems measured by 15N addition experiments: Total uptake. *Limnology and Oceanography*, *54*(3), 653-665. http://pubs.er.usgs.gov/publication/70034854

He, J., Poder, T., Dupras, J., & Enomana, H. J. (2016). La valeur économique de la pêche blanche et des services écosystémiques au Lac Saint-Pierre: analyse coûts-avantages des stratégies d'adaptation aux changements climatiques. Rapport présenté à la Division des impacts et de l'adaptation liés aux changements climatiques de Ressources naturelles Canada, au Gouvernement du Québec et à Ouranos. Montréal: Université du Québec à Montréal.

Heffernan, J. B., & Cohen, M. J. (2010). Direct and indirect coupling of primary production and diel nitrate dynamics in a subtropical spring-fed river. *Limnology and Oceanography*, *55*(2), 677-688. https://doi.org/10.4319/lo.2010.55.2.0677

Hilt, S. (2015). Regime shifts between macrophytes and phytoplankton–concepts beyond shallow lakes, unravelling stabilizing mechanisms and practical consequences. *Limnetica*, *34*(2), 467-480.

Hilt, S., Brothers, S., Jeppesen, E., Veraart, A. J., & Kosten, S. (2017). Translating Regime Shifts in Shallow Lakes into Changes in Ecosystem Functions and Services. *BioScience*, *67*(10), 928-936. https://doi.org/10.1093/biosci/bix106

Howarth, R., Swaney, D., Billen, G., Garnier, J., Hong, B., Humborg, C., . . . Marino, R. (2012). Nitrogen fluxes from the landscape are controlled by net anthropogenic nitrogen inputs and by climate. *Frontiers in Ecology and the Environment*, *10*(1), 37-43. https://doi.org/https://doi.org/10.1890/100178

Howarth, R. W., Billen, G., Swaney, D., Townsend, A., Jaworski, N., Lajtha, K., . . . Zhao-Liang, Z. (1996). Regional nitrogen budgets and riverine N & P fluxes for the drainages to the North Atlantic Ocean: Natural and human influences. *Biogeochemistry*, *35*(1), 75-139. https://doi.org/10.1007/BF02179825

Huang, N. E., Shen, Z., Long, S. R., Wu, M. C., Shih, H. H., Zheng, Q., . . . Liu, H. H. (1998). The empirical mode decomposition and the Hilbert spectrum for nonlinear and non-stationary time series analysis. *Proceedings of the Royal Society of London. Series A: Mathematical, Physical and Engineering Sciences*, *454*(1971), 903-995. https://doi.org/doi:10.1098/rspa.1998.0193

Hudon, C. (1997). Impact of water level fluctuations on St. Lawrence River aquatic vegetation. *Canadian Journal of Fisheries and Aquatic Sciences*, *54*(12), 2853-2865. https://doi.org/doi:10.1139/f97-201

Hudon, C., Armellin, A., Gagnon, P., & Patoine, A. (2010). Variations in water temperatures and levels in the St. Lawrence River (Québec, Canada) and potential implications for three common fish species. *Hydrobiologia*, *647*(1), 145-161. https://doi.org/10.1007/s10750-009-9922-6

1028 Hudon, C., & Carignan, R. (2008). Cumulative impacts of hydrology and human
1029 activities on water quality in the St. Lawrence River (Lake Saint-Pierre, Quebec, Canada)
1030 [Article]. *Canadian Journal of Fisheries and Aquatic Sciences*, *65*(6), 1165-1180.
1031 https://doi.org/10.1139/f08-069

1032 Hudon, C., Gagnon, P., Rondeau, M., Hébert, S., Gilbert, D., Hill, B., . . . Starr, M.
1033 (2017). Hydrological and biological processes modulate carbon, nitrogen and phosphorus flux
1034 from the St. Lawrence River to its estuary (Quebec, Canada). *Biogeochemistry*, *135*(3), 251-276.
1035 https://doi.org/10.1007/s10533-017-0371-4

1036 Hudon, C., Jean, M., & Létourneau, G. (2018). Temporal (1970–2016) changes in human
1037 pressures and wetland response in the St. Lawrence River (Québec, Canada). *Science of The*
1038 *Total Environment*, *643*, 1137-1151.
1039 https://doi.org/https://doi.org/10.1016/j.scitotenv.2018.06.080

1040 Hudon, C., Lalonde, S., & Gagnon, P. (2000). Ranking the effects of site exposure, plant
1041 growth form, water depth, and transparency on aquatic plant biomass. *Canadian Journal of*
1042 *Fisheries and Aquatic Sciences*, *57*(S1), 31-42.

1043 Hudon, C., Wilcox, D., & Ingram, J. (2006). Modeling wetland plant community
1044 response to assess water-level regulation scenarios in the Lake Ontario-St. Lawrence River basin.
1045 *Environmental Monitoring and Assessment*, *113*(1-3), 303-328. https://doi.org/10.1007/s10661-
1046 005-9086-4

1047 James, W. F. (2010). Nitrogen retention in a floodplain backwater of the upper
1048 Mississippi River (USA). *Aquatic Sciences*, *72*(1), 61-69. https://doi.org/10.1007/s00027-009-
1049 0113-3

1050 Jean, M., Létourneau, G., & Savage, C. (2002). Freshwater wetland and exotic plant
1051 species 2nd edition. In S. a. T. B. Environment Canada, Water Quality Monitoring (Ed.),
1052 *Monitoring sheet in the "Monitoring of the State of the St. Lawrence" series.*

1053 Johnson, J. B., & Omland, K. S. (2004). Model selection in ecology and evolution.
1054 *Trends in Ecology & Evolution*, *19*(2), 101-108.
1055 https://doi.org/https://doi.org/10.1016/j.tree.2003.10.013

1056 Karjalainen, H., Stefansdottir, G., Tuominen, L., & Kairesalo, T. (2001). Do submersed
1057 plants enhance microbial activity in sediment? *Aquatic Botany*, *69*(1), 1-13.

1058 Kim, K., & Oh, H.-S. (2018). EMD: Empirical Mode Decomposition and Hilbert Spectral
1059 Analysis. R package version 1.5.8.

1060 Kimber, A., Valk, A. G. v. d., & Korschgen, C. E. (1995). The distribution of Vallisneria
1061 americana seeds and seedling light requirements in the Upper Mississippi River. *Canadian*
1062 *Journal of Botany*, *73*(12), 1966-1973. https://doi.org/10.1139/b95-210

1063 Lacoul, P., & Freedman, B. (2006). Environmental influences on aquatic plants in
1064 freshwater ecosystems. *Environmental Reviews*, *14*(2), 89-136. https://doi.org/10.1139/a06-001

1065 Lehmann, M. F., Barnett, B., Gélinas, Y., Gilbert, D., Maranger, R. J., Mucci, A., . . .
1066 Thibodeau, B. (2009). Aerobic respiration and hypoxia in the Lower St. Lawrence Estuary:
1067 Stable isotope ratios of dissolved oxygen constrain oxygen sink partitioning. *Limnology and*
1068 *Oceanography*, *54*(6), 2157-2169. https://doi.org/https://doi.org/10.4319/lo.2009.54.6.2157

1069 Lloyd, C. E. M., Freer, J. E., Collins, A. L., Johnes, P. J., & Jones, J. I. (2014). Methods
1070 for detecting change in hydrochemical time series in response to targeted pollutant mitigation in
1071 river catchments. *Journal of Hydrology*, *514*, 297-312.
1072 https://doi.org/https://doi.org/10.1016/j.jhydrol.2014.04.036

1073 Lu, C., Zhang, J., Tian, H., Crumpton, W. G., Helmers, M. J., Cai, W.-J., . . . Lohrenz, S.
1074 E. (2020). Increased extreme precipitation challenges nitrogen load management to the Gulf of
1075 Mexico. *Communications Earth & Environment*, *1*(1), 21. https://doi.org/10.1038/s43247-020-
1076 00020-7

1077 Madsen, J. D., Chambers, P. A., James, W. F., Koch, E. W., & Westlake, D. F. (2001).
1078 The interaction between water movement, sediment dynamics and submersed macrophytes.
1079 *Hydrobiologia*, *444*(1), 71-84. https://doi.org/10.1023/A:1017520800568

1080 Mitsch, W. J., Day, J. W., Wendell Gilliam, J., Groffman, P. M., Hey, D. L., Randall, G.
1081 W., & Wang, N. (2001). Reducing nitrogen loading to the Gulf of Mexico from the Mississippi
1082 River Basin: strategies to counter a persistent ecological problem. *BioScience*, *51*(5), 373-388.

Morin, J., & Côté, J.-P. (2003). Modifications anthropiques sur 150 ans au lac Saint-Pierre: une fenêtre sur les transformations de l'écosystème du Saint-Laurent. *VertigO*, *4*(3). https://doi.org/10.4000/vertigo.3867

Morse, B. (1990). St. Lawrence River water levels study: Application ot the One-D hydrodynamic model. Transport Canada, Waterways Development Division, Canadian Coast Guard.

Mulholland, P. J., Tank, J. L., Webster, J. R., Bowden, W. B., Dodds, W. K., Gregory, S. V., . . . Wollheim, W. M. (2002). Can uptake length in streams be determined by nutrient addition experiments? Results from an interbiome comparison study. *Journal of the North American Benthological Society*, *21*(4), 544-560. https://doi.org/10.2307/1468429

Newbold, J. D., Elwood, J. W., O'Neill, R. V., & Winkle, W. V. (1981). Measuring nutrient spiralling in streams. *Canadian Journal of Fisheries and Aquatic Sciences*, *38*(7), 860-863.

Nijssen, B., O'Donnell, G. M., Hamlet, A. F., & Lettenmaier, D. P. (2001). Hydrologic Sensitivity of Global Rivers to Climate Change. *Climatic Change*, *50*(1), 143-175. https://doi.org/10.1023/A:1010616428763

Oksanen, J., Blanchet, F. G., Friendly, M., Kindt, R., Legendre, P., McGlinn, D., . . . H, W. (2020). vegan: Community Ecology Package. R package version 2.5-7. https://CRAN.R-project.org/package=vegan

Ouranos. (2015). Vers l'adaptation. Synthèse des connaissances sur les changements climatiques au Québec. Édition 2015. Montréal, Québec: Ouranos.

Peterson, B. J., Wollheim, W. M., Mulholland, P. J., Webster, J. R., Meyer, J. L., Tank, J. L., . . . Hershey, A. E. (2001). Control of nitrogen export from watersheds by headwater streams. *Science*, *292*(5514), 86-90.

Phillips, D. L., & Gregg, J. W. (2001). Uncertainty in source partitioning using stable isotopes. *Oecologia*, *127*(2), 171-179. https://doi.org/10.1007/s004420000578

Piña-Ochoa, E., & Álvarez-Cobelas, M. (2006). Denitrification in Aquatic Environments: A Cross-system Analysis. *Biogeochemistry*, *81*(1), 111-130. https://doi.org/10.1007/s10533-006-9033-7

Pinardi, M., Bartoli, M., Longhi, D., Marzocchi, U., Laini, A., Ribaudo, C., & Viaroli, P. (2009). Benthic metabolism and denitrification in a river reach: a comparison between vegetated and bare sediments. *Journal of Limnology*, *68*(1), 133-145. https://doi.org/10.4081/jlimnol.2009.133

Pinheiro, J., Bates, D., DebRoy, S., Sarkar, D., & RCoreTeam. (2020). nlme: Linear and nonlinear mixed effects models. R package version 3.1-144. https://CRAN.R-project.org/package=nlme

Preiner, S., Dai, Y., Pucher, M., Reitsema, R. E., Schoelynck, J., Meire, P., & Hein, T. (2020). Effects of macrophytes on ecosystem metabolism and net nutrient uptake in a groundwater fed lowland river. *Science of The Total Environment*, *721*, Article 137620. https://doi.org/10.1016/j.scitotenv.2020.137620

R Core Team. (2020). R: A language and environment for statistical computing. R Foundation for Statistical Computing, Vienna, Austria. https://www.R-project.org/

Rice, S. P., Kiffney, P., Greene, C., & Pess, G. R. (2008). The ecological importance of tributaries and confluences. *River confluences, tributaries and the fluvial network*, 209-242.

Riis, T., Olesen, B., Clayton, J. S., Lambertini, C., Brix, H., & Sorrell, B. K. (2012). Growth and morphology in relation to temperature and light availability during the establishment of three invasive aquatic plant species. *Aquatic Botany*, *102*, 56-64. https://doi.org/10.1016/j.aquabot.2012.05.002

Rooney, N., & Kalff, J. (2000). Inter-annual variation in submerged macrophyte community biomass and distribution: the influence of temperature and lake morphometry. *Aquatic Botany*, *68*(4), 321-335.

Runkel, R., & De Cicco, L. (2017). Rloadest: River Load Estimation. R package version 0.4.5.

Scheffer, M., Hosper, S. H., Meijer, M. L., Moss, B., & Jeppesen, E. (1993). Alternative equilibria in shallow lakes. *Trends in Ecology & Evolution*, *8*(8), 275-279. https://doi.org/https://doi.org/10.1016/0169-5347(93)90254-M

Seitzinger, S., Harrison, J. A., Böhlke, J. K., Bouwman, A. F., Lowrance, R., Peterson, B., . . . Drecht, G. V. (2006). Denitrification across landscapes and waterscapes: a synthesis.

Ecological Applications, *16*(6), 2064-2090. https://doi.org/https://doi.org/10.1890/1051-0761(2006)016[2064:DALAWA]2.0.CO;2

Seitzinger, S. P., Styles, R. V., Boyer, E. W., Alexander, R. B., Billen, G., Howarth, R. W., . . . van Breemen, N. (2002). Nitrogen retention in rivers: model development and application to watersheds in the northeastern U.S.A. *Biogeochemistry*, *57*(1), 199-237. https://doi.org/10.1023/A:1015745629794

Short, F. T., Kosten, S., Morgan, P. A., Malone, S., & Moore, G. E. (2016). Impacts of climate change on submerged and emergent wetland plants. *Aquatic Botany*, *135*, 3-17. https://doi.org/https://doi.org/10.1016/j.aquabot.2016.06.006

Stallone, A., Cicone, A., & Materassi, M. (2020). New insights and best practices for the successful use of Empirical Mode Decomposition, Iterative Filtering and derived algorithms. *Scientific Reports*, *10*(1), 15161. https://doi.org/10.1038/s41598-020-72193-2

Stream Solute Workshop. (1990). Concepts and Methods for Assessing Solute Dynamics in Stream Ecosystems. *Journal of the North American Benthological Society*, *9*(2), 95-119. https://doi.org/10.2307/1467445

Tall, L., Caraco, N., & Maranger, R. (2011). Denitrification hot spots: dominant role of invasive macrophyte Trapa natans in removing nitrogen from a tidal river. *Ecological Applications*, *21*(8), 3104-3114. http://www.jstor.org/stable/41417114

Tank, J. L., Rosi-Marshall, E. J., Baker, M. A., & Hall, R. O. (2008). Are Rivers Just Big Streams? A Pulse Method to Quantify Nitrogen Demand in a Large River. *Ecology*, *89*(10), 2935-2945. http://www.jstor.org/stable/27650838

Teng, W., Rui, H., Strub, R., & Vollmer, B. (2016). Optimal Reorganization of NASA Earth Science Data for Enhanced Accessibility and Usability for the Hydrology Community. *JAWRA Journal of the American Water Resources Association*, *52*(4), 825-835. https://doi.org/https://doi.org/10.1111/1752-1688.12405

Thieurmel, B., & Elmarhraoui, A. (2019). Suncalc: Compute sun position, sunlight phase and Lunar Phase. R package version 0.0.5. https://CRAN.R-project.org/package=suncalc

Van Meter, K. J., Chowdhury, S., Byrnes, D. K., & Basu, N. B. (2020). Biogeochemical asynchrony: Ecosystem drivers of seasonal concentration regimes across the Great Lakes Basin. *Limnology and Oceanography*, *65*(4), 848-862. https://doi.org/https://doi.org/10.1002/lno.11353

Venables, W. N., & Ripley, B. D. (2002). Modern Applied Statistics with S. Fourth Edition. Springer, New York.

Vis, C. (2004). Importance relative des producteurs primaires sur la production globale du lac Saint-Pierre, un grand lac fluvial du Saint-Laurent. PhD Thesis, Université de Montréal, Montréal, CA. https://papyrus.bib.umontreal.ca/xmlui/handle/1866/15024

Vis, C., Hudon, C., Carignan, R., & Gagnon, P. (2007). Spatial analysis of production by macrophytes, phytoplankton and epiphyton in a large river system under different water-level conditions. *Ecosystems*, *10*(2), 293-310. https://doi.org/10.1007/s10021-007-9021-3

von Schiller, D., Bernal, S., & Martí, E. (2011). Technical Note: A comparison of two empiricalapproaches to estimate in-stream net nutrient uptake. *Biogeosciences*, *8*(4), 875-882. https://doi.org/10.5194/bg-8-875-2011

Wollheim, W. M., Voosmarty, C. J., Peterson, B. J., Seitzinger, S. P., & Hopkinson, C. S. (2006). Relationship between river size and nutrient removal. *Geophysical Research Letters*, *33*(6), Article L06410. https://doi.org/10.1029/2006gl025845

Wu, Z., & Huang, N. E. (2009). Ensemble empirical mode decomposition: a noise-assisted data analysis method. *Advances in Adaptive Data Analysis*, *01*(01), 1-41. https://doi.org/10.1142/s1793536909000047

Wu, Z., Huang, N. E., Long, S. R., & Peng, C.-K. (2007). On the trend, detrending, and variability of nonlinear and nonstationary time series. *Proceedings of the National Academy of Sciences*, *104*(38), 14889-14894. https://doi.org/10.1073/pnas.0701020104

Ye, S., Reisinger, A. J., Tank, J. L., Baker, M. A., Hall, R. O., Rosi, E. J., & Sivapalan, M. (2017). Scaling Dissolved Nutrient Removal in River Networks: A Comparative Modeling Investigation. *Water Resources Research*, *53*(11), 9623-9641. https://doi.org/10.1002/2017wr020858

Zuur, A. F., Ieno, E. N., Walker, N. J., Saveliev, A. A., & Smith, G. M. (2009). *Mixed Effects Models and Extensions in Ecology with R*. Springer Science+Business Media.